

Using these DNAs, sequence analysis was performed in P, F₁ and F₂ between black and mutant mice. Sequence analysis of 6 P (3 blacks and 3 mutants), 3 F₁ and 12 F₂ (9 blacks (2 homos and 7 heteros) and 3 mutants) showed that phenotype and genotype were completely coincident, indicating that this novel mutation is regulated by the *ru2^d* allele (data not shown).

RT-PCR analysis of P, F₁ and F₂ using primers inside exons 9 and 11 (Fig. 2A) revealed that the long form was mainly detected in *+/+* genotype, the short form in *ru2^d/ru2^d* and intermediate pattern in *+/ru2^d* (Fig. 2B). These results suggest that the *ru2^d* mutation reduces mRNA expression of the long form of the *Hps5* gene.

Proliferation and differentiation of *ru2^d/ru2^d* melanocytes

There was no difference in the proliferation of melanoblasts derived from epidermal cell suspension cultured in MDM between *+/+* (Fig. 3A) and *ru2^d/ru2^d* (Figs. 3B and 4A) mice. Melanocyte differentiation was similarly limited in MDM between the two mice (Fig. 4D). In contrast, processes of *ru2^d/ru2^d* melanoblasts (Fig. 3B) were shorter than those of *+/+* melanoblasts (Fig. 3A). In MDMM, no difference was also observed in melanoblast/melanocyte proliferation between *+/+* and *ru2^d/ru2^d* mice (Fig. 4B), whereas melanocyte differentiation in *ru2^d/ru2^d* mice was greatly inhibited (Figs. 3D, 4E) compared to that in *+/+* mice (Fig. 3C). Only 5% of *ru2^d/ru2^d* cells were differentiated melanocytes with low pigmentation and dendricity. In MDMD, similarly, no difference was observed in melanoblast/melanocyte proliferation between *+/+* and *ru2^d/ru2^d* mice (Figs. 5A, C, 6A, B), whereas melanocyte differentiation in *ru2^d/ru2^d* mice was greatly inhibited compared to that in *+/+* mice (Fig. 6C, D). Only 10% of *ru2^d/ru2^d* cells were differentiated melanocytes with low pigmentation and dendricity. In MDMDF, there was also no difference in melanoblast proliferation between *+/+* (Figs. 3E, 4C) and *ru2^d/ru2^d* (Fig. 3F) mice, whereas melanocyte differentiation in *ru2^d/ru2^d* mice was inhibited compared to that in *+/+* mice (Fig. 4F). Moreover, processes of *ru2^d/ru2^d* melanoblasts (Fig. 3F) were slightly shorter than those of *+/+* melanoblasts (Fig. 3E). These results suggest that the *ru2^d* mutation greatly inhibits melanocyte differentiation, pigmentation and dendritogenesis.

Effects of L-Tyr on the proliferation and differentiation of *ru2^d/ru2^d* melanocytes in vitro and in vivo

Since hypopigmented melanocytes such as pink-eyed dilution (*p*) melanocytes were induced to proliferate and differentiate to pigmented melanocytes by adding excess L-Tyr to culture media (Hirobe et al., 2002), the hypopigmented *ru2^d/ru2^d* melanocytes were thought to be induced to proliferate and differentiate similarly. The proliferation of *+/+* melanocytes in MDMD was greatly inhibited by additional L-Tyr in a concentration-dependent

manner (Fig. 6A), while the proliferation of *ru2^d/ru2^d* melanoblasts and melanocytes was not (Fig. 6B), suggesting that the proliferation of fully differentiated melanocytes is inhibited by excess L-Tyr, but not the proliferation of melanoblasts and melanocytes with low pigmentation. In contrast, melanocyte differentiation was stimulated by L-Tyr in a concentration-dependent manner both in *+/+* (Fig. 6C) and *ru2^d/ru2^d* (Fig. 6D) mice, while the stimulation of melanocyte differentiation in *ru2^d/ru2^d* melanocytes was much greater than in *+/+* melanocytes (Fig. 6C, D). The proportion of differentiated *ru2^d/ru2^d* melanocytes in the cultures added with L-Tyr at concentrations of 1 and 2 mM exceeded 90% after 14 days (Fig. 6D). Differentiated melanocytes with enlarged cytoplasm and increased pigmentation were observed both in *+/+* (Fig. 5B) and *ru2^d/ru2^d* (Fig. 5D) mice. However, the

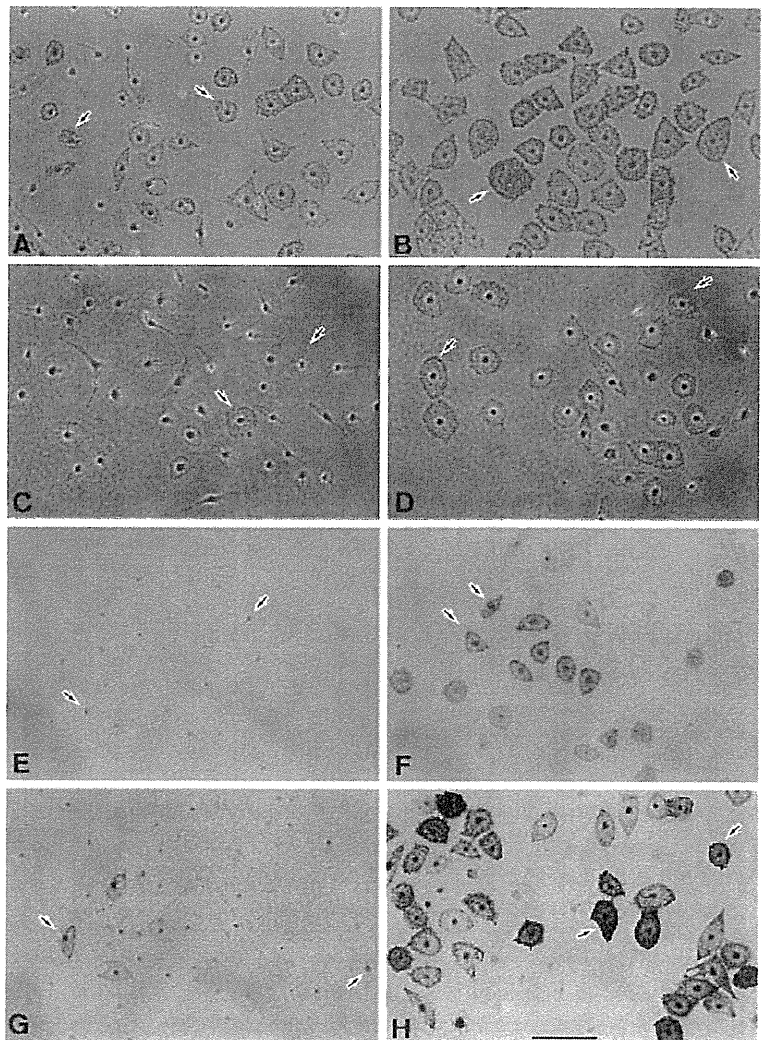


Fig. 5. Melanoblasts and melanocytes in pure cultures derived from epidermal cell suspensions of 0.5-day-old *+/+* (A, B) and *ru2^d/ru2^d* (C–H) mice for 14 days in MDMD with (B, D, F, H) or without (A, C, E, G) L-Tyr (2 mM). Dopa (E, F) and dopa-premelanin (G, H) reactions were performed. Differentiated melanocytes derived from *+/+* (A) and *ru2^d/ru2^d* (C) are dendritic, polygonal or epithelioid (arrows). L-Tyr increased the pigmentation both in *+/+* (B) and *ru2^d/ru2^d* (D) melanocytes and the reactivity to dopa (F) and dopa-premelanin (H) of *ru2^d/ru2^d* melanocytes (arrows). A–D, Phase-contrast microscopy. E–H, Bright-field microscopy. Scale bar, 100 μ m.

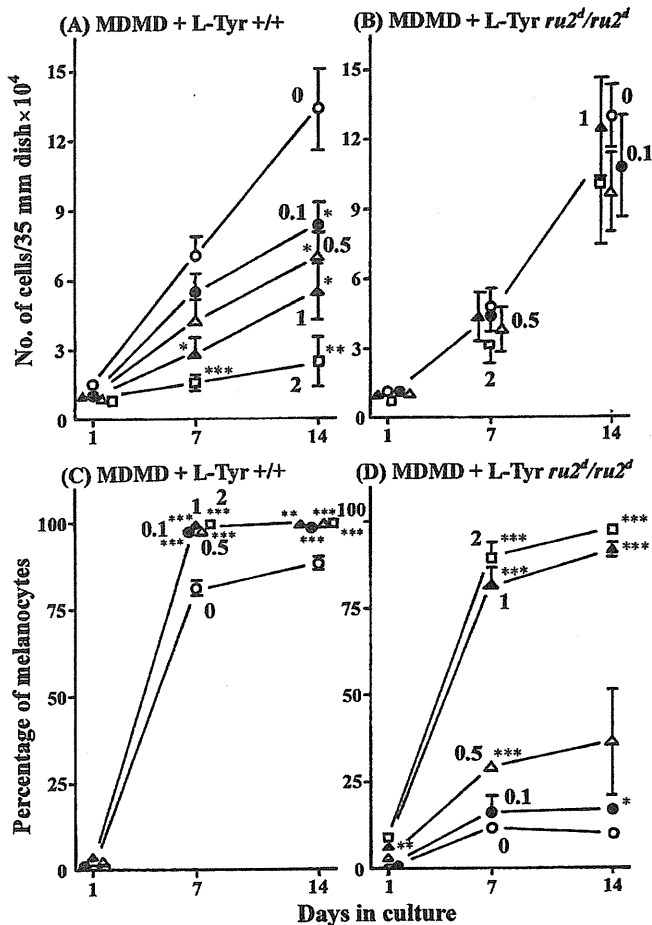


Fig. 6. Kinetics of the proliferation (A, B) and differentiation (C, D) of +/+ (A, C) and $ru2^d/ru2^d$ (B, D) melanocytes cultured in MDMD with or without (○) L-Tyr at various concentrations of 0.1 (●), 0.5 (△), 1 (▲) and 2 (□) mM for 14 days. Protocols are as detailed for Fig. 4. * $P < 0.05$.

pigmentation in +/+ melanocytes was much greater than in $ru2^d/ru2^d$ melanocytes.

Newborn $ru2^d/ru2^d$ mice were injected with L-Tyr everyday and fixed at 6.5 days. The number of dopa-positive melanocytes dramatically increased after treatment with L-Tyr (Table 3), exceeding control at 6.5 days ($P < 0.01$). The melanocytes possessed well-developed dendrites in addition to dopa-melanin depositions in cell body. On the other hand, no change was observed in the number of melanoblasts/melanocytes positive to the combined dopa-premelanin reaction after treatment with L-Tyr (Table 3), suggesting that the treatment with L-Tyr leads to the differentiation of melanoblasts to melanocytes. In contrast, no change was observed in the number of melanocytes and melanoblasts/melanocytes of +/+ mice after treatment with L-Tyr (Table 3).

Dopa and premelanin reactions of $ru2^d/ru2^d$ melanoblasts and melanocytes in vitro

When epidermal cell suspensions derived from +/+ and $ru2^d/ru2^d$ mice were cultured in MDMD for 14 days, the percentage of dopa-positive melanocytes in the melanoblast-melanocyte population of +/+ (98.46%) and $ru2^d/ru2^d$ (49.85%) skin was greater than the percentage of pig-

Table 3. Effects of L-Tyr on the proliferation and differentiation of B10-+/+ and B10- $ru2^d/ru2^d$ melanocytes in vivo. The number of epidermal melanocytes (cells positive to the dopa reaction) and melanoblasts plus melanocytes (cells positive to the combined dopa-premelanin reaction) in the dorsal skin of B10-+/+ and B10- $ru2^d/ru2^d$ mice after treatment with L-Tyr (1 mM) in vivo. Skin samples were fixed at 6.5 days. The number of melanocytes in $ru2^d/ru2^d$ mice was dramatically increased by the injection of L-Tyr. The data are averages of results from three experiments \pm S.E.M. **shows statistical difference (** $P < 0.01$).

Experiment	Number of melanocytes/0.1 mm ² epidermis	Number of melanoblasts and melanocytes/0.1 mm ² epidermis
B10-+/+, control	36.36 \pm 3.85	60.42 \pm 9.35
B10-+/+, L-Tyr	48.07 \pm 5.98	67.61 \pm 4.18
B10- $ru2^d/ru2^d$, control	7.77 \pm 0.73	63.38 \pm 3.30
B10- $ru2^d/ru2^d$, L-Tyr	46.06 \pm 8.17**	65.32 \pm 5.04

Table 4. Cells positive to the dopa reaction and to the combined dopa-premelanin reaction of cultured melanoblasts and melanocytes derived from B10-+/+ and B10- $ru2^d/ru2^d$ mice. Epidermal cell suspensions derived from 0.5-day-old B10-+/+ and B10- $ru2^d/ru2^d$ mice were cultured with MDMD with or without L-Tyr (2 mM) for 14 days. Dopa and combined dopa-premelanin reactions were performed as written in Materials and Methods. The data are averages of results from three experiments \pm standard errors of the mean (S.E.M.). Each experiment was performed with different litters of mice. **,***shows statistical difference (** $P < 0.01$, *** $P < 0.001$) between +/+ and $ru2^d/ru2^d$.

Reaction	Medium	Percentage of positive cells	
		B10-+/+	B10- $ru2^d/ru2^d$
Dopa	MDMD	98.46 \pm 0.13	49.85 \pm 5.47***
	MDMD + L-Tyr	99.27 \pm 0.41	97.55 \pm 1.33
Dopa + Ag	MDMD	99.80 \pm 0.20	69.22 \pm 4.45***
	MDMD + L-Tyr	99.23 \pm 0.54	97.39 \pm 1.47

mented melanocytes in the melanoblast-melanocyte population (87.85% for +/+ mice and 9.56% for $ru2^d/ru2^d$ mice), suggesting that many populations of non-pigmented but dopa-reactive cells exist in $ru2^d/ru2^d$ mice (Table 4). Dopa-melanin depositions in $ru2^d/ru2^d$ melanocytes was greatly reduced and restricted to the area around nucleus (Fig. 5E). However, L-Tyr (2 mM) greatly increased dopa-melanin depositions all over the cytoplasm of $ru2^d/ru2^d$ melanocytes (arrows; Fig. 5F). Silver depositions after the combined dopa-premelanin reaction in cultured $ru2^d/ru2^d$ melanoblasts and melanocytes (indicated by arrow in the right side; Fig. 5G) was weak and restricted to the area around the nucleus, except for a few cells (indicated by arrow in the left side; Fig. 5G) with full silver depositions all over the cytoplasm. However, L-Tyr dramatically increased silver depositions all over the cytoplasm in cultured $ru2^d/ru2^d$ melanoblasts and melanocytes (arrows; Fig. 5H). These results suggest that TYR activity and melanosome formation and maturation in $ru2^d/ru2^d$ melanocytes are greatly inhibited, but that the inhibition can be relieved, at least in part, by excess L-Tyr.

Immunocytochemistry of cultured $ru2^d/ru2^d$ melanocytes

Expression of TYR, TRP1 (Fig. 7B) and TRP2 (Fig. 7D) in $ru2^d/ru2^d$ melanoblasts and melanocytes cultured in

MDMD was lower than that of TYR, TRP1 (Fig. 7A) and TRP2 (Fig. 7C) in *+/+* melanocytes, whereas Kit expression was not different (Table 5). Similar pattern of expression of TRP1, TRP2 and Kit were observed in both *+/+* and *ru2^d/ru2^d* melanoblasts cultured in MDMD, but TYR expression was not observed in either strain (Table 5). L-Tyr (2 mM) stimulated expression of TYR (Fig. 8A), TRP1 (Fig. 8B), TRP2 (Fig. 8C) and Kit (Fig. 8D) in *ru2^d/ru2^d* melanoblasts and melanocytes (Table 5).

Melanin content in cultured melanocytes and culture media

PTCA content in *ru2^d/ru2^d* melanocytes cultured in MDMD was much lower (> 19-fold) than in *+/+* melanocytes (Fig. 9A), whereas its content in culture media was greater (> 3-fold) than in *+/+* melanocytes (Fig. 9B). L-Tyr (2 mM) dramatically (> 7-fold) increased PTCA content in culture media derived from *ru2^d/ru2^d* melanocytes, although no increase was observed in culture media derived from *+/+* melanocytes even in the presence of excess L-Tyr (Fig. 9B). In contrast, 4-AHP content in cultured *ru2^d/ru2^d* melanocytes did not differ from that in *+/+* melanocytes (Fig. 9C). L-Tyr elicited a more than 2.5-fold increase in 4-AHP content both in *+/+* and *ru2^d/ru2^d* melanocytes in a similar fashion (Fig. 9C). The content of 4-AHP in culture media derived from *ru2^d/ru2^d* melanocytes did not differ from that of *+/+* melanocytes. Although treatment with L-Tyr increased 4-AHP content in culture media derived from both *ru2^d/ru2^d* and *+/+* melanocytes, the stimulation in culture media derived from *ru2^d/ru2^d* melanocytes was much lower than in *+/+* melanocytes (Fig. 9D).

Electron microscopy of melanosomes and other organelles of *ru2^d/ru2^d* melanocytes

Melanosomes present in cultured *+/+* melanocytes (Fig. 10A) were exclusively elliptical or ovoid with longitudinal depositions of pigments in intraluminal fibrils and mostly in stage IV. In *ru2^d/ru2^d* melanocytes, melanosomes in similar morphology with intraluminal fibrils were also observed, but many immature stage III melanosomes and less stage IV melanosomes were observed (Fig. 10C). The number of stage III melanosomes in *ru2^d/ru2^d* melanocytes did not differ from that of *+/+* melanocytes (Fig. 11), whereas the number of stage IV melanosomes was much smaller (> 47-fold; Fig. 11). The total number of melanosomes in *ru2^d/ru2^d* melanocytes was also smaller than in *+/+* melanocytes (> 2-fold, Fig. 11). In *ru2^d/ru2^d* melanocytes, well-developed Golgi apparatus and many mitochondria were observed (Fig. 10C). The difference in the number of Golgi apparatus between *ru2^d/ru2^d* and *+/+* melanocytes was statistically significant (Fig. 12). Treatment with L-Tyr markedly increased the number of stage IV melanosomes and the total number of melanosomes in *ru2^d/ru2^d* melanocytes (Fig. 11B), whereas the treatment decreased the

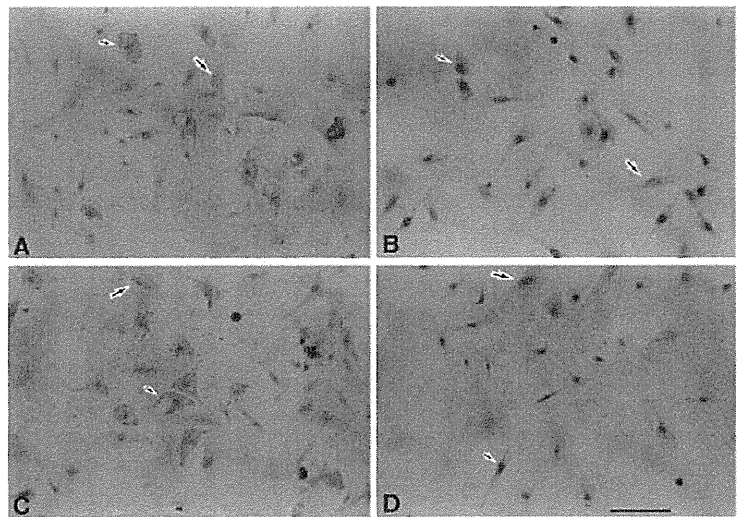


Fig. 7. Immunocytochemical stainings of cultured melanoblasts and melanocytes from *+/+* (A, C) and *ru2^d/ru2^d* (B, D) mice cultured in MDMD for 7 days. TRP1 (A, B) and TRP2 (C, D) stainings are shown. Melanocytes (small arrows) are reactive, but keratinocytes (large arrows) are not reactive in both mice. Bright-field microscopy. Scale bar, 100 μ m.

Table 5. Immunocytochemical stainings of cultured melanoblasts and melanocytes derived from B10-*+/+* and B10-*ru2^d/ru2^d* mice. Epidermal cell suspensions derived from 0.5-day-old B10-*+/+* and B10-*ru2^d/ru2^d* mice were cultured with MDMD, MDMD + L-Tyr (2 mM) and MDMDF for seven days. The epidermal cell suspensions of three different groups were derived from the same litter of mice. Similar results were obtained from three experiments. Each experiment was performed with different litters of mice. -, negative; \pm , negative/positive; +, positive; ++, strong; +++, intense; +++++, very intense.

Gene	Medium	TYR	TRP1	TRP2 (DCT)	Kit
<i>+/+</i>	MDMD	+	+++	+++	+
	MDMD + L-Tyr	+	++++	++++	++
	MDMDF	-	+++	+++	+
<i>ru2^d/ru2^d</i>	MDMD	\pm	++	+	+
	MDMD + L-Tyr	+	+++	++	++
	MDMDF	-	++	+	+

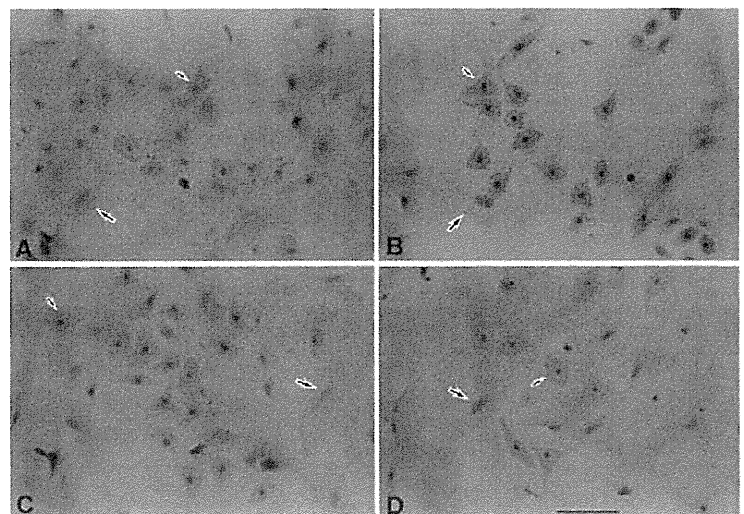


Fig. 8. Immunocytochemical stainings of *ru2^d/ru2^d* melanocytes cultured in MDMD added with L-Tyr (2 mM) for 7 days. TYR (A), TRP1 (B), TRP2 (C) and Kit (D) stainings are shown. Melanocytes (small arrows) are reactive, but keratinocytes (large arrows) are not reactive. Bright-field microscopy. Scale bar, 100 μ m.

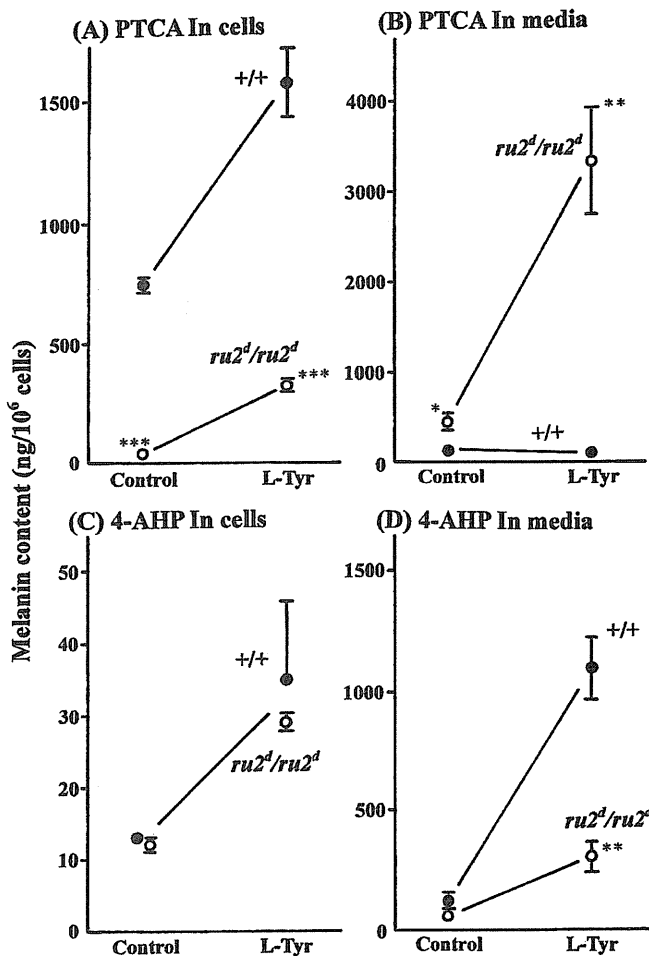


Fig. 9. PTCA (A, B) and 4-AHP (C, D) contents in cultured melanocytes (A, C) and culture media (B, D) from 0.5-day-old *+/+* and *ru2^d/ru2^d* mice with or without L-Tyr (2 mM). Samples of culture media were derived from 10–20 dishes during the two days from days 12 to 14. Samples of cell homogenates were also derived from 10–20 dishes. **P* < 0.05, ***P* < 0.01, ****P* < 0.001.

number of stage II melanosomes in *ru2^d/ru2^d* (Fig. 11B). Treatment with L-Tyr decreased the number of stage III melanosomes in *+/+* melanocytes (Fig. 11A). Moreover, treatment with L-Tyr decreased the number of Golgi apparatus (Fig. 12A) and mitochondria (Fig. 12B) both in *+/+* and *ru2^d/ru2^d* melanocytes, but not of lysosomes (Fig. 12C). These results suggest that the *ru2^d* mutation inhibits melanosome formation and maturation, but its impaired melanosome formation and that maturation can be rescued by excess L-Tyr.

DISCUSSION

Mouse *Hps5* gene is on chromosome 7 and possesses a 3381-bp ORF with 23 exons, encoding an 1126-amino acid protein (127.4 kDa), 81% homologies to the human sequence (126.3 kDa) are observed (Zhang et al., 2003). All tissues (heart, brain, spleen, lung, liver, skeletal muscle, kidney and testes) examined contained the 4.8 kb transcript. Nine murine mutations in the *Hps5* (*Ru2*) gene have been identified to present: the *ru2^{mr}* (*Hps5^{ru2-mr}*) allele is a spontaneous recessive mutation with undefined molecular characterization (Bateman, 1957); the *ru2^{hz}* (*Hps5^{ru2-hz}*) allele leads to a predicted loss of 118 C-terminal aa (frameshift by insertion of CCGG at E900) (Dickie, 1965; Zhang et al., 2003); the *ru2* (*Hps5^{ru2}*) allele contains a 1.0-kb insertion (K867) of the H2A histone sequence immediately preceding codon 868 of exon 18 (Lilly, 1966; Zhang et al., 2003); the *ru2^J* (*Hps5^{ru2-J}*) allele leads to a predicted loss of 311 aa at the C terminus (frameshift by Δ G757) (Eicher, 1977; Zhang et al., 2003); the *ru2^{8J}* (*Hps5^{ru2-8J}*) allele is a spontaneous recessive mutation with undefined molecular characterization (Cook, 1995); the *ru2^{11J}* (*Hps5^{ru2-11J}*) allele is an N-ethyl-N-nitrosourea (ENU)-induced recessive mutation with undefined molecular characterization (Gwynn et al., 2004, Mouse Genome Informatics); the *ru2^{Btlr}* (*Hps5^{ru2-Btlr}*) allele leads to T- to C transition in the donor splice site of intron 9 (ENU-induced recessive mutation) (Eidendchenk et al., 2008 in Mouse Genome Informatics); and the *ru2^{2Btlr}* (*Hps5^{ru2-2Btlr}*) allele leads to A- to T- transversion at nucleotide position 2337 (ENU-induced recessive mutation) (Blasius et al., 2008 in Mouse Genome Informatics).

In the present study, we first reported the tenth allele occurred in mice, *ru2^d* (*Hps5^{ru2-d}*), caused by frameshift by deletion (Δ G997). The *ru2^d* mutation makes large molecule protein to smaller one by a premature termination codon, and reduces mRNA expression. The expression of the long form mRNA in *ru2^d/ru2^d* mice was lower than that in *+/+* mice. Although the precise mechanism of this phenomenon is not

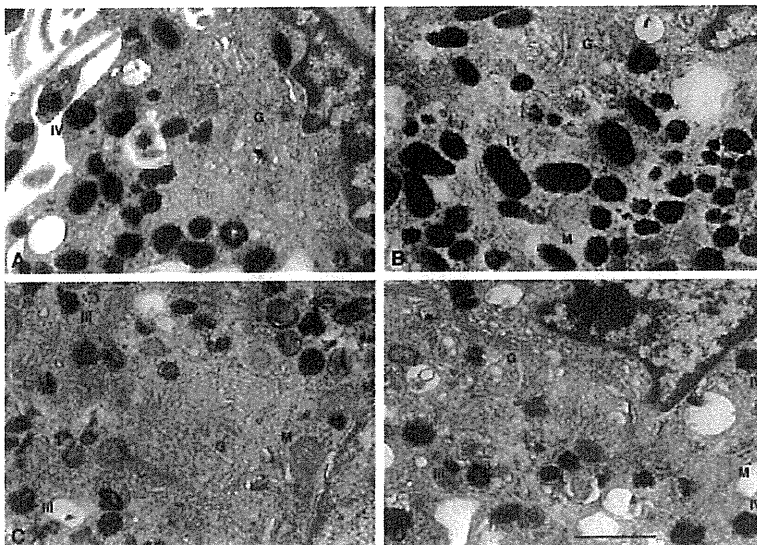


Fig. 10. Electron micrographs of four epidermal melanocytes from *+/+* (A, B) and *ru2^d/ru2^d* (C, D) mice cultured in MDMD with (B, D) or without (A, C) L-Tyr (2 mM) for 14 days. Numerous stage IV (IV) melanosomes are seen in *+/+* melanocyte (A). In contrast, *ru2^d/ru2^d* melanocyte possesses only a few stage IV melanosomes but numerous stage III (III) melanosomes in addition to well-developed Golgi apparatus (G) and mitochondria (M). Numerous stage IV melanosomes are seen in *+/+* and *ru2^d/ru2^d* melanocytes by treatment with L-Tyr. Scale bar, 0.5 μ m.

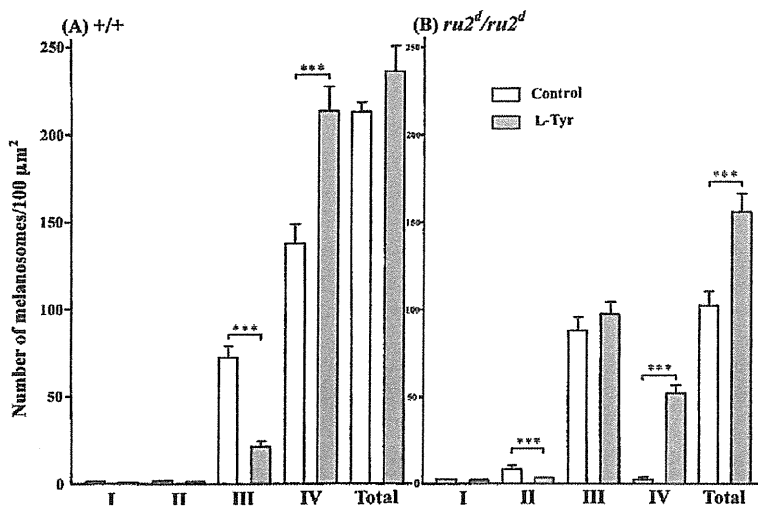


Fig. 11. The number of stage I, II, III and IV melanosomes as well as the total number of melanosomes in cultured +/+ (A) and *ru2^d/ru2^d* (B) melanocytes with or without L-Tyr (2 mM). The differences in the number of stage II and IV melanosomes as well as the total number of melanosomes between +/+ and *ru2^d/ru2^d* are statistically significant. The differences in the number of stage III and IV melanosomes between control cells and L-Tyr-treated cells in +/+ mice are also statistically significant. The differences in the number of stage II and IV melanosomes as well as the total number of melanosomes between control cells and L-Tyr-treated cells in *ru2^d/ru2^d* mice are also statistically significant (****P* < 0.001).

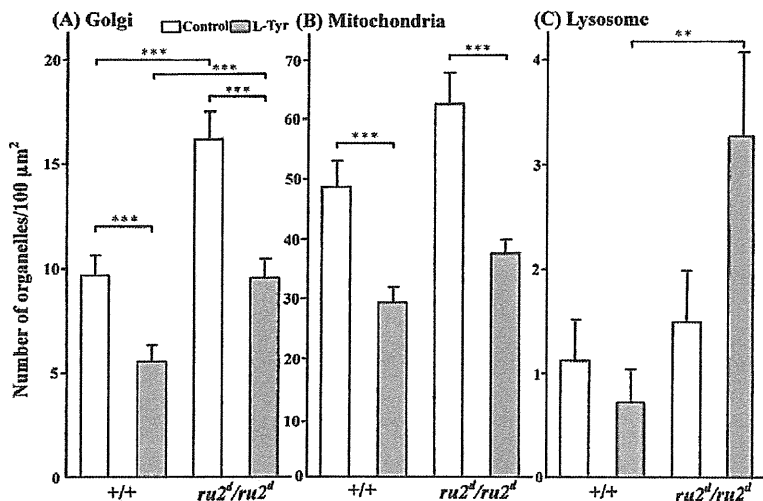


Fig. 12. Changes in the number of the Golgi apparatus (A), mitochondria (B) and lysosome (C) in cultured +/+ and *ru2^d/ru2^d* melanocytes with or without L-Tyr (2 mM). The number of the Golgi apparatus in *ru2^d/ru2^d* melanocytes is greater than in +/+ melanocytes (****P* < 0.001). L-Tyr reduced the number of the Golgi apparatus in both +/+ and *ru2^d/ru2^d* melanocytes. The number of mitochondria in *ru2^d/ru2^d* melanoblasts/melanocytes is greater than in +/+ melanocytes, although this difference is not statistically significant. L-Tyr decreased the number of mitochondria of both +/+ and *ru2^d/ru2^d* melanocytes (****P* < 0.001). The number of lysosomes in +/+ and *ru2^d/ru2^d* melanocytes showed no notable change, except that its number in *ru2^d/ru2^d* melanocytes treated with L-Tyr is greater than that of +/+ melanocytes treated with L-Tyr (***P* < 0.01).

known, it might be possible that the efficiency of splicing of the long form mRNA was reduced by the deletion mutation and the efficiency of splicing of the short form mRNA was increased. Another possibility is that the efficiency of splicing of the short form mRNA was increased by the degradation

of the long form mRNA through nonsense-mediated mRNA decay (NMD) in the long form owing to the premature termination codon. It is thought that the efficiency of splicing of the short form mRNA was not increased by NMD, but the premature termination codon resulted in the increase in the relative ratio of the short form mRNA to the long form mRNA by the degradation of the long form mRNA through NMD.

Human *HPS1*, 2, 3, 4, 7 and 8 correspond to mouse pale ear (*ep*), pearl (*pl*), cocoa (*coa*), light ear (*le*), sandy (*sd*) and reduced pigmentation (*rp*), respectively (Wei, 2006). All the *Hps* mutations are characterized by hypopigmentation and several diseases, and in mice, *Hps* is a disorder of organelle biogenesis in which hypopigmentation, bleeding, and pulmonary fibrosis are resulted from defects in melanosomes, platelet dense granules and lysosomes (Wei, 2006). The difference in the coat color in the *Hps* mutant seems to be due to the inhibition of melanosome formation (inner structure) and maturation. Zhang et al. (2003) reported that in the retinal pigment epithelium and choroid of C57BL/6J (B6)-*ru2/ru2* mice, melanosomes were fewer and immature, and their shapes were mostly spherical. Nguyen et al. (2002) reported that in the hair follicle melanocytes of dorsal skin of 4-week-old B6-*ru2/ru2* mice, stage IV melanosomes also decreased in number, and their morphology remained spherical. However, in the present study, *ru2^d/ru2^d* melanosomes were elliptical, but they were fewer and immature, suggesting that the *ru2^d* allele controls the maturation of melanosomes, but not their internal structure. The severity of the lesion in *ru2^d* allele (melanosome formation and maturation) may be less than that of *ru2* allele.

Our present study demonstrated that *ru2^d/ru2^d* melanoblasts possess a greater number of Golgi apparatus than do +/+ melanocytes. The Golgi apparatus in +/+ melanocytes in the epidermis of newborn mice are known to decrease in number with greater developmental age (Hirobe and Takeuchi, 1978). Since melanosomes are at least in part originated from the Golgi apparatus (Seiji et al., 1963; Novikoff et al., 1968; Maul, 1969; Imokawa and Mishima, 1981; Hirobe, 1982), Golgi apparatus is thought to gradually decrease in number with increasing formation of melanosomes. In this study, L-Tyr did reduce the number of Golgi apparatus in +/+ and *ru2^d/ru2^d* melanoblasts/melanocytes. Since in +/+ melanocytes, the formation and maturation of melanosomes are fully activated, a small number of the Golgi apparatus is thought to exist in normal circumstances. In contrast, since in *ru2^d/ru2^d* melanoblasts, the formation and maturation of melanosomes are not fully activated, the Golgi apparatus is thought to be well-developed. Moreover, since melanosome formation and maturation was stimulated by L-Tyr in *ru2^d/ru2^d* melanoblasts/melanocytes, the Golgi apparatus is thought to exist in a similar number as that of +/+ melanocytes. Therefore, it is possible that the Golgi apparatus in

ru2^d/ru2^d melanoblasts is developed more greatly than in +/+ melanocytes due to their reduced melanosome formation and maturation.

HPS proteins associate with other HPS proteins to form complexes or Biogenesis of Lysosome-related Organelles Complexes (BLOCs, Li et al., 2004). HPS proteins participate as components of one of the three heteromeric BLOC complexes (BLOC-1, -2 and -3; Li et al., 2004). The proteins encoded by the pallid (*pa*), mutated (*mu*), cappuccino (*cno*) and sandy (*sdyl/Hps7^{sdyl}*) genes form the 200–230 kDa BLOC-1 complex (Gwynn et al., 2004; Li et al., 2004). The proteins encoded by the cocoa (*coa/Hps3^{coa}*), ruby-eye 2 (*ru2/Hps5^{ru2}*) and ruby-eye (*ru/Hps6^{ru}*) genes form 350 kDa BLOC-2 complex (Di Pietro et al., 2004; Gautam et al., 2004; Gwynn et al., 2004; Li et al., 2004; Setty et al., 2007), while the proteins encoded by the pale ear (*ep/Hps1^{ep}*) and light ear (*le/Hps4^{le}*) genes form 175 kDa BLOC-3 complex (Li et al., 2004). HPS proteins function in complexes to mediate the synthesis of several lysosome-related organelles such as melanosome, platelet dense granule, lung lamellar body and lytic granule (Li et al., 2004). It is possible that the *ru2^d* (*Hps5^{ru2-d}*) allele affects the function of BLOC-2, followed by inhibition of melanosome maturation, rather than inhibition of the formation of melanosome inner structure, as the *ru2^d* allele failed to inhibit the formation of melanosome inner structure in this study. In fact, in cultured human melanocytes derived from patients of HPS-3 (Boissy et al., 2005) and -5 (Helip-Wooley et al., 2007), TYR, TRP1 and/or TRP2 were aberrantly trafficked, and maturation of melanosomes was inhibited despite their normal inner structures. These results suggest that proteins forming BLOC-2 complex are involved in regulating the trafficking of TYR, TRP1, TRP2 molecules, and in delivering to melanosomes followed by the increase in melanin synthesis.

Alpha-MSH induces mouse melanocyte differentiation in vivo (Hirobe and Takeuchi, 1977a, 1978) and in vitro (Hirobe and Takeuchi, 1977b; Hirobe, 1992c) by stimulating the activity of TYR, TRP1, TRP2 and Kit, eumelanin synthesis and melanosome formation and maturation through the cAMP–protein kinase A (PKA) signaling pathway (Hirobe, 2005). Melanocyte differentiation was limited in *ru2^d/ru2^d* mice, even in the presence of α -MSH or DBcAMP, whereas melanocytes could be induced to differentiate by excess L-Tyr in vitro and in vivo. These results suggest that α -MSH–cAMP–PKA signaling pathway could be functioning fine, but the step requiring *Ru2* function occurs downstream. Therefore, it is reasonable to conclude that untreated *ru2^d/ru2^d* melanocytes cannot differentiate, but that they are able to do so at high L-Tyr levels.

Eumelanin content in cultured *ru2^d/ru2^d* melanocytes was much lower (> 19-fold) than in +/+ melanocytes, but the reduction of eumelanin content in *ru2^d/ru2^d* melanocytes was recovered by treatment with L-Tyr (> 5-fold). Surprisingly, eumelanin content in culture media derived from *ru2^d/ru2^d* melanocytes treated with (> 25-fold) or without (> 3.5-fold) L-Tyr was much greater than that of +/+ melanocytes. These results suggest that *ru2^d/ru2^d* melanocytes can synthesize much more eumelanin by excess L-Tyr, but that it is difficult for eumelanin to accumulate in melanosomes. Thus, it is possible that the *ru2^d* allele affects the mechanisms of accumulation of eumelanin in melanosomes. The

pink-eyed dilution (*p*) mutation also greatly inhibits TYR, TRP1, and TRP2 activity, eumelanin synthesis and melanosome formation and maturation (Hirobe et al., 2002), but the inhibition by the *p* allele is much greater than by the *ru2^d* allele. Moreover, the rescue of eumelanin synthesis by L-Tyr in *p/p* melanocytes is much more limited than in *ru2^d/ru2^d* melanocytes. Eumelanin produced by excess L-Tyr in *p/p* melanocytes is also released to culture media (Hirobe et al., 2002). It is possible that the low activity of eumelanin accumulation in *ru2^d/ru2^d* melanocytes is caused by the acidity of melanosomes, similar to *p/p* melanocytes (Hirobe et al., 2002).

Pheomelanin content in *ru2^d/ru2^d* melanocytes cultured with or without L-Tyr was similar to that in +/+ melanocytes. Although pheomelanin content in culture media derived from *ru2^d/ru2^d* melanocytes did not differ from that of +/+ melanocytes, increase in pheomelanin content in culture media derived from L-Tyr-treated *ru2^d/ru2^d* melanocytes was much lower than that of +/+ melanocytes. These results suggest that the *ru2^d* allele does not affect pheomelanogenesis in normal circumstances, and overproduction and release of pheomelanin in excess L-Tyr conditions are not observed.

ACKNOWLEDGMENTS

The authors express their thanks to Dr. Hearing (NIH, Bethesda, MD, USA) for providing the antibodies for TYR, TRP1 and TRP2 and to Dr. Nishikawa (RIKEN, Kobe, Japan) for Kit. This work was in part supported by Grants-in-Aid for Scientific Research (No. 18591262 and 20591357) from Japan Society for the Promotion of Science (to SI, WK and HT).

ACCESSION NUMBER

Transcript variant 1 mRNA (NM_001005247) of Hermansky-Pudlak syndrome 5 homolog protein short-form variant, EntryID, AB598691, 20101104173541.41408.

REFERENCES

- Bateman N (1957) Maroon – allele of silver? *Mouse News Lett* 16: 7
- Bennett DC, Lamoreux ML (2003) The color loci of mice – a genetic century. *Pigment Cell Res* 16: 333–344
- Boissy RE, Richmond B, Huizing M, Helip-Wooley A, Zhao Y, Koshoffer A, et al. (2005) Melanocyte-specific proteins are aberrantly trafficked in melanocytes of Hermansky-Pudlak syndrome-Type 3. *Am J Pathol* 165: 231–240
- Cook S (1995) Spontaneous remutation (*ru2^{BJ}*). *Mouse Genome* 93: 862
- Cooksey CJ, Garratt PJ, Land EJ, Pavel S, Ramsden CA, Riley PA, et al. (1997) Evidence of the indirect formation of the catecholic intermediate substrate responsible for the autoactivation kinetics of tyrosinase. *J Biol Chem* 272: 89–96
- Dickie MM (1965) Haze. *Mouse News Lett* 32: 44
- Di Pietro SM, Falcon-Perez JM, Dell'Angelica EC (2004) Characterization of BLOC-2, a complex containing the Hermansky-Pudlak syndrome proteins HPS3, HPS5 and HPS6. *Traffic* 5: 276–283
- Eicher EM, Fox S (1977) hz and mr alleles of ru-2. *Mouse News Lett* 56: 42
- Fitzpatrick TB, Hori Y, Toda K, Seiji M (1969) Melanin 1969: some definitions and problems. *Jpn J Dermatol (Ser B)* 79: 278–282
- Gautam R, Chintala S, Li W, Zhang Q, Tan J, Novak EK, et al. (2004) The Hermansky-Pudlak syndrome 3 (cocoa) protein is a component of the Biogenesis of Lysosome-related Organelles Complex-2 (BLOC-2). *J Biol Chem* 279: 12935–12942
- Gwynn B, Martina JA, Bonifacio JS, Sviderskaya EV, Lamoreux

- ML, Bennett DC, et al. (2004) Reduced pigmentation (*rp*), a mouse model of Hermansky-Pudlak syndrome, encodes a novel component of the BLOC-1 complex. *Blood* 15: 3181–3189
- Hearing VJ (2000) The melanosome: the perfect model for cellular response to the environment. *Pigment Cell Res* 13 (Suppl 8): 23–34
- Hearing VJ, Tsukamoto K (1991) Enzymatic control of pigmentation in mammals. *FASEB J* 5: 2902–2909
- Helip-Wooley A, Westbrook W, Dorward HM, Koshoffer A, Huizing M, Boissy RE, et al. (2007) Improper trafficking of melanocyte-specific proteins in Hermansky-Pudlak syndrome type-5. *J Invest Dermatol* 127: 1471–1478
- Hirobe T (1982) Origin of melanosome structures and cytochemical localizations of tyrosinase activity in differentiating epidermal melanocytes of newborn mouse skin. *J Exp Zool* 224: 355–363
- Hirobe T (1984) Histochemical survey of the distribution of the epidermal melanoblasts and melanocytes in the mouse during fetal and postnatal periods. *Anat Rec* 208: 589–594
- Hirobe T (1992a) Control of melanocyte proliferation and differentiation in the mouse epidermis. *Pigment Cell Res* 5: 1–11
- Hirobe T (1992b) Basic fibroblast growth factor stimulates the sustained proliferation of mouse epidermal melanoblasts in a serum-free medium in the presence of dibutyl cyclic AMP and keratinocytes. *Development* 114: 435–445
- Hirobe T (1992c) Melanocyte stimulating hormone induces the differentiation of mouse epidermal melanocytes in serum-free culture. *J Cell Physiol* 152: 337–345
- Hirobe T (2005) Role of keratinocyte-derived factors involved in regulating the proliferation and differentiation of mammalian epidermal melanocytes. *Pigment Cell Res* 18: 2–12
- Hirobe T (2011) How are proliferation and differentiation of melanocytes regulated? *Pigment Cell Melanoma Res* 24: 462–478
- Hirobe T, Abe H (1999) Genetic and epigenetic control of the proliferation and differentiation of mouse epidermal melanocytes in culture. *Pigment Cell Res* 12: 147–163
- Hirobe T, Abe H (2007) Changes of melanosome morphology associated with the differentiation of epidermal melanocytes in slaty mice. *Anat Rec* 290: 981–993
- Hirobe T, Takeuchi T (1977a) Induction of melanogenesis in the epidermal melanoblasts of newborn mouse skin by MSH. *J Embryol Exp Morphol* 37: 79–90
- Hirobe T, Takeuchi T (1977b) Induction of melanogenesis *in vitro* in the epidermal melanoblasts of newborn mouse skin by MSH. *In Vitro* 13: 311–315
- Hirobe T, Takeuchi T (1978) Changes of organelles associated with the differentiation of epidermal melanocytes in the mouse. *J Embryol Exp Morphol* 43: 107–121
- Hirobe T, Wakamatsu K, Ito S (1998) Effects of genic substitution at the agouti, brown, albino, dilute, and pink-eyed dilution loci on the proliferation and differentiation of mouse epidermal melanocytes in serum-free culture. *Eur J Cell Biol* 75: 184–191
- Hirobe T, Wakamatsu K, Ito S, Abe H, Kawa Y, Mizoguchi M (2002) Stimulation of the proliferation and differentiation of mouse pink-eyed dilution epidermal melanocytes by excess tyrosine in serum-free primary culture. *J Cell Physiol* 191: 162–172
- Imokawa G, Mishima Y (1981) Isolation and biochemical characterization of tyrosinase-rich GERL and coated vesicle in melanin synthesizing cells. *Brit J Dermatol* 104: 169–178
- Ito S (2003) A chemist's view of melanogenesis. *Pigment Cell Res* 16: 230–236
- Ito S, Fujita K (1985) Microanalysis of eumelanin and pheomelanin in hair and melanomas by chemical degradation and liquid chromatography. *Anal Biochem* 144: 527–536
- Ito S, Wakamatsu K (1994) An improved modification of permanganate oxidation of eumelanin that gives a constant yield of pyrrole-2,3,5-tricarboxylic acid. *Pigment Cell Res* 7: 141–144
- Ito S, Wakamatsu K (2008) Chemistry of mixed melanogenesis – pivotal roles of dopaquinone. *Photochem Photobiol* 84: 582–592
- Jackson IJ, Chambers DM, Rinchik EM, Bennett DC (1990) Characterisation of TRP-1 mRNA levels in dominant and recessive mutations at the mouse brown locus. *Genetics* 126: 451–456
- Jackson IJ, Chambers DM, Tsukamoto K, Copeland NG, Gilbert DM, Jenkins NA, et al. (1992) A second tyrosinase-related protein, TRP-2 maps to and is mutated at the mouse slaty locus. *EMBO J* 11: 527–535
- Kawa Y, Ito M, Ono H, Asano M, Takano N, Ooka S, et al. (2000) Stem cell factor and/or endothelin-3 dependent immortal melanoblast and melanocyte populations derived from mouse neural crest cells. *Pigment Cell Res* 13 (Suppl 8): 73–80
- Korner AM, Pawelek J (1980) DOPAchrome conversion: a possible control point in melanin biosynthesis. *J Invest Dermatol* 75: 192–195
- Lamoureux ML, Delmas V, Larue L, Bennett DC (2010) The Colors of Mice. A Model Genetic Network. Wiley-Blackwell, Oxford
- Li W, Rusiniak ME, Chintala S, Gautam R, Novak EK, Swank RT (2004) Murine Hermansky-Pudlak syndrome genes: regulators of lysosome-related organelles *BioEssays* 26: 616–628
- Lilly F (1966) The genetic basis of susceptibility and resistance of mice to the Gross and Friend leukemia viruses. *Mouse News Lett* 34: 14
- Maul GG (1969) Golgi-melanosome relationship in human melanoma *in vitro*. *J Ultrastruct Res* 26: 163–176
- Mayer TC (1973) The migratory pathway of neural crest cells into the skin of mouse embryos. *Dev Biol* 34: 39–46
- Nguyen T, Novak EK, Kermani M, Fluhr J, Peters LL, Swank RT, et al. (2002) Melanosome morphologies in murine models of Hermansky-Pudlak syndrome reflect blocks in organelle development. *J Invest Dermatol* 119: 1156–1164
- Novikoff AB, Alabara A, Biempica L (1968) Ultrastructural and cytochemical observations on B-16 and Harding-Passey mouse melanomas. The origin of premelanosomes and compound melanosomes. *J Histochem Cytochem* 16: 299–319
- Ozeki H, Ito S, Wakamatsu K, Hirobe T (1995) Chemical characterization of hair melanins in various coat-color mutants of mice. *J Invest Dermatol* 105: 361–364
- Rawles ME (1947) Origin of pigment cells from the neural crest in the mouse embryo. *Physiol Zool* 20: 248–266
- Seiji M, Shimao K, Birbeck MSC, Fitzpatrick TB (1963) Subcellular localization of melanin biosynthesis. *Ann N Y Acad Sci* 100: 497–533
- Setty SRG, Tenza D, Truschel ST, Chou E, Sviderskaya EV, Theos AC, et al. (2007) BLOC-1 is required for cargo-specific sorting from vacuolar early endosomes toward lysosome-related organelles. *Mol Biol Cell* 18: 768–780
- Silvers WK (1979) *The Coat Colors of Mice*. (Berlin: Springer-Verlag Press)
- Tsukamoto K, Jackson IJ, Urabe K, Montague P, Hearing VJ (1992) A melanogenic enzyme termed DOPAchrome tautomerase is a novel tyrosinase-related protein, TRP-2. *EMBO J* 11: 527–535
- Wakamatsu K, Ito S, Rees JL (2002) The usefulness of 4-amino-3-hydroxyphenylalanine as a specific marker of pheomelanin. *Pigment Cell Res* 15: 225–232
- Wei ML (2006) Hermansky-Pudlak syndrome: a disease of protein trafficking and organelle function. *Pigment Cell Res* 19: 19–42
- Zhang Q, Zhao B, Li W, Oiso N, Novak EK, Rusiniak ME, et al. (2003) *Ru2* and *Ru* encode mouse orthologs of the genes mutated in human Hermansky-Pudlak syndrome types 5 and 6. *Nature Genetics* 33: 145–153

(Received March 7, 2011 / Accepted April 25, 2011)

電気化学計測技術を応用した ヒト卵丘細胞-卵子複合体の呼吸能解析

阿部宏之* 吉田仁秋**

本症例では、走査型電気化学顕微鏡を用いてヒトの卵丘細胞-卵子複合体 (COC) の呼吸活性と卵子成熟能の関係を調べた。卵丘細胞が多層に付着している COC は呼吸量が大きく、卵丘細胞には発達したミトコンドリアが多数存在し、卵丘細胞と卵子間にはギャップ結合が観察された。一方、卵丘細胞が剥離している COC は呼吸活性が低く、卵丘細胞のミトコンドリアは小型で数も少なかった。卵子の成熟率は卵丘細胞が多数付着している COC ほど高い傾向にあった。

はじめに

走査型電気化学顕微鏡 (scanning electrochemical microscopy; SECM) を用いた電気化学計測 (イメージング) 法は、局所領域における生物反応を電気化学的に高精度で検出できる有効な技術である。筆者らは、高感度マイクロ電極、非侵襲呼吸測定液、多検体測定プレートなど呼吸測定に関する独自の要素技術を開発し、SECM をベースにこれら要素技術を有機的にシステム化した「受精卵呼吸測定装置」を開発している。これまでに「受精卵呼吸測定装置」を用いて、マウス、ウシ、ブタ、ヒトの単一胚の酸素消費量 (呼吸量) を無侵襲的に測定することに成功し、胚の品質 (クオリティー) と呼吸活性が密接に関係していることを明らかにしている¹⁾。このように精度の高い呼吸測定技術は、呼吸活性を指標に胚や卵子の品質を評価するための極めて有効な方法となる。そこで本研究では、「受精卵呼吸測定装置」を用いてヒト卵

丘細胞-卵子複合体 (cumulus-oocyte complex; COC) の酸素消費量 (呼吸量) を計測し、COC の呼吸活性と卵丘細胞および卵子の超微形態、成熟培養による卵子成熟率との関係を調べた結果について報告する。

1. 症 例

1 材 料

不妊治療の終了により余剰となり、学術研究への使用に対して患者の同意が得られた COC を呼吸量測定に供した。

2 呼吸量測定

COC の呼吸量は、SECM をベースに開発した「受精卵呼吸測定装置」(図 1a) を用いて測定した。個々の COC を測定専用プレート (図 1b) のマイクロウェル底部中心に静置した後、酸素の還元電位を検出する微小電極を透明帯近傍に移動した。本測定に用いたマイクロ電極は、計測感度を上げるために先端径 2~5 μm にエッチングした白金電極をガラスキャピラリー

* Hiroyuki Abe 山形大学大学院理工学研究科バイオ化学工学専攻

** Hiroaki Yoshida 吉田レディースクリニック

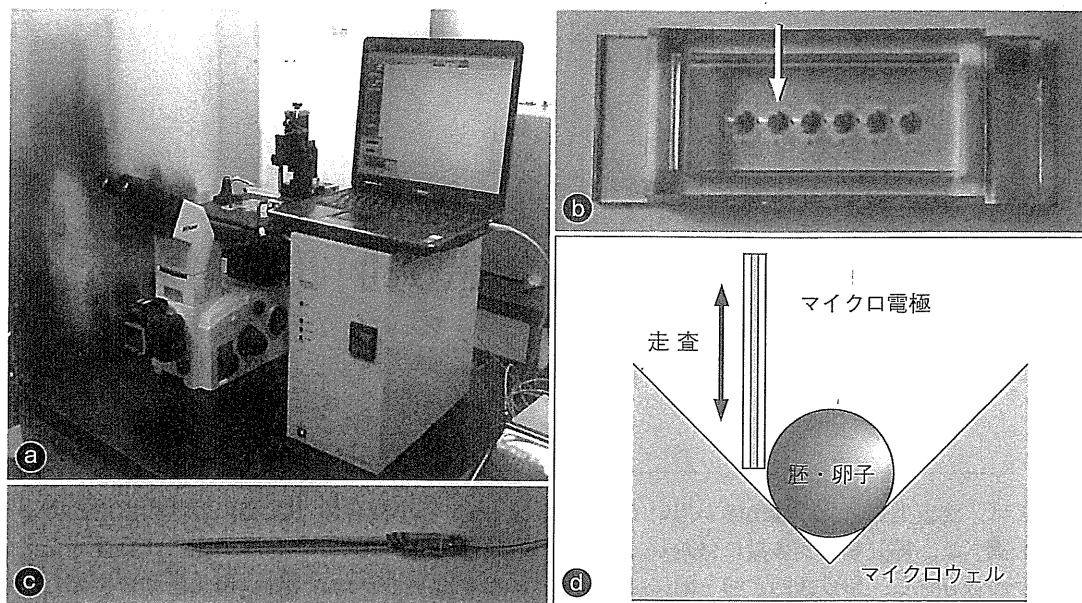


図1

a: 走査型電気化学顕微鏡を改良した「受精卵呼吸測定装置」。倒立型顕微鏡, ポテンショスタット, ノートパソコン (呼吸能解析ソフトを内蔵) で構成される。b: 多検体測定プレート; プレート底面には円錐形のマイクロウェルが6穴施されている。c: 呼吸測定用マイクロ電極; ディスク型白金マイクロ電極で, 先端部が直径 2~5 μm にエッチング加工された白金電極がガラスキャピラリーに熱封止されている。d: マイクロウェル底部に試料 (胚または卵子) を静置した後, マイクロ電極を胚に対して鉛直方向に走査することで酸素消費量を測定する。

に封止したディスク型電極 (図1c) を使用した。マイクロ電極は, 酸素が還元可能な -0.6 V vs Ag/AgCl に保持し, 鉛直方向に移動速度 $31\ \mu\text{m}/\text{秒}$, 走査距離 $160\ \mu\text{m}$ の条件で試料近傍を走査し酸素の還元電流を測定した (図1d)。胚の酸素消費量は, 球面拡散理論式に基づいた専用の解析ソフトを用いて算出した。

3 COC の呼吸量

不妊治療において採取されたCOCを卵丘細胞層と卵子の形態的特徴を基準に次の5つのグレードに分類した (図2)。卵丘細胞が4層以上に密に付着しているCOCをグレード1, 卵丘細胞が1~3層付着しているCOCをグレード2, 卵丘細胞に覆われる領域が1/2以下のCOCをグレード3のカテゴリーに分類した。一方, 卵丘細胞がまったく付着していない完全裸化卵子をグレード4, 卵丘細胞が少数付着し卵子が変形しているものをグレード5のカテゴリーとした。

各グレードのCOCの酸素消費量を「受精卵呼吸測定装置」を用いて測定した結果, 卵丘細胞が最も多く付着しているグレード1の平均酸素消費量 ($\times 10^{14}/\text{mol} \cdot \text{sec}^{-1}$) は7.79と最大を示した (表1)。一方, グレード2およびグレード3の酸素消費量は, それぞれ1.46および1.26と卵丘細胞の減少に伴い酸素消費量が低下し, グレード4とグレード5ではさらに少ない酸素消費量が計測された。このように, COCの呼吸活性は卵子の付着している卵丘細胞の数に大きく影響することが示された。

4 COC の微細構造観察

ミトコンドリアは酸化リン酸化反応 (呼吸) によって細胞活動に必須のエネルギー (ATP) を産生している。ミトコンドリアは呼吸機能の変化に伴い顕著な形態的变化を示すことから, 呼吸量計測の有用性を検証するためには, 卵子や卵丘細胞のミトコンドリアの微細構造解析は極めて重要である。そこで, 各グレードのCOC

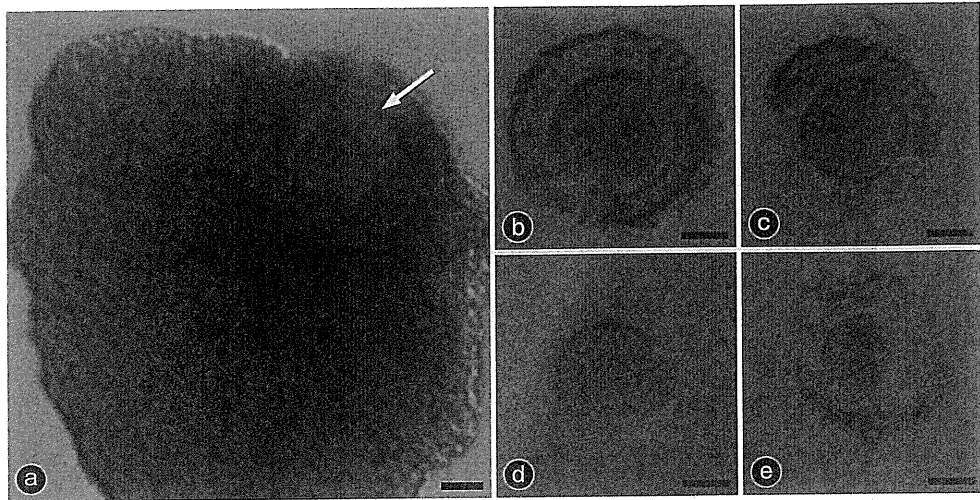


図2 COCの光学顕微鏡像
 a: グレード1; 卵子(⇒)の周囲には卵丘細胞層が多層に密に付着している。b: グレード2; 卵丘細胞が1~3層付着している。c: グレード3; 卵丘細胞層は1~3層で部分的に剥離している。d: グレード4; 卵丘細胞がまったく付着していない。e: グレード5; 卵丘細胞層の付着が認められるが卵子が変形している。スケールバーは、50 μmを示す。

表1 形態的特徴(グレード1~5)により分類したCOCの酸素消費量

カテゴリー	酸素消費量 ($F \times 10^{14} / \text{mol} \cdot \text{sec}^{-1}$)
グレード1	7.79 ± 1.00 (50)
グレード2	1.46 ± 0.15 (25)
グレード3	1.26 ± 0.35 (8)
グレード4	0.86 ± 0.30 (2)
グレード5	0.77 (1)

括弧内の数字は、測定した試料の数を示す。

においてミトコンドリアを中心とする細胞小器官の微細構造を電子顕微鏡により観察した。呼吸測定したCOCの一部をグルタルアルデヒドおよびオスミック酸で固定した後、定法に従いエポキシ樹脂に包埋し超薄切片を作製し、透過型電子顕微鏡で微細構造観察を行った。グレード1のCOCでは、卵丘細胞において拡張したクリステを持つミトコンドリアが多数存在し、卵丘細胞と卵子の間には典型的なギャップ結合が数多く観察された(図3a, b)。卵子には、円形で小型のミトコンドリアが多数存在し、それらの多くはクラスターを形成し細胞質にほぼ均一に分布していた(図3c)。一方、グレード2およびグレード3のCOCでは、卵丘細胞内のミトコンドリアはグレード1のCOCと比べて

小型で数も少なく、また、多くのミトコンドリアはクリステが未発達であった(図3d, e)。グレード1で観察された卵丘細胞と卵子とのギャップ結合は、グレード2およびグレード3のCOCではほとんど認められなかった。卵子のミトコンドリアについては、数や形態、分布様式などグレード間での顕著な違いは認められなかった。

5 COCの形態と卵子成熟率の関係

ヒトのCOCは、卵丘細胞の付着状態を基準に分類したグレードによって、呼吸量やミトコンドリアの微細形態が顕著に異なることが明らかとなった。ミトコンドリアやギャップ結合は卵子の成長や成熟に重要な役割を果たしていると考えられることから、本研究では各グレードのCOCを成熟培養し、卵子の成熟能にグレード間の違いがあるのか検討した。COCをTCM199培地に10%患者血清(patient's serum)、ヒト絨毛性性腺刺激ホルモン(human chorionic gonadotropin; HCG) 100IU/ml、卵胞刺激ホルモン(follicle stimulating hormone; FSH) 75 IU/mlを加えた培養液を用いて37°C、5% CO₂ in airの条件で26時間、成熟培養を行った。その結果、卵子成熟率はグレー

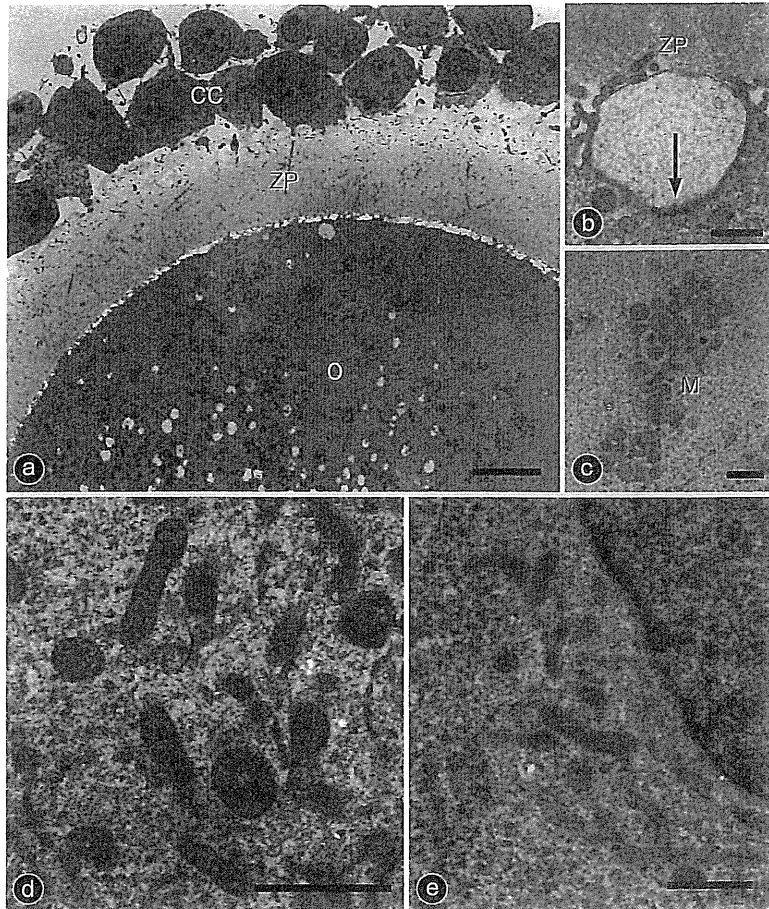


図3 COCの電子顕微鏡像

a~d: グレード1。卵細胞表面には卵丘細胞から伸びた突起との間にギャップ結合(⇒)が観察される(b)。卵子(O)には円形で小型のミトコンドリア(M)がクラスター状になって、ほぼ均一に局在している(a, c)。卵丘細胞にはクリステが発達したミトコンドリアが多数観察される(d)。e: グレード3。卵丘細胞のミトコンドリアは小型で数も少ない。ZP: 透明帯。スケールバーは、a: 10 μm, b~e: 1 μmを示す。

ド1で70.0%, グレード2で63.3%, グレード3で20.0%, グレード4で33.3%, グレード5で0%でありグレード間に卵子成熟率の違いが認められた(図4)。

2. 考 察

細胞の酸素消費量測定をもとにした胚の呼吸量測定は、Cartesian diver法²⁾、分光光度法(spectrophotometrics)^{3)~5)}、ピレンなど蛍光物質を用いた蛍光発色法(fluorescence)^{6)~8)}などが報告されている。しかし、これらの方法は計測感度が低く、侵襲的な方法であることから、

一般的には普及していない。非侵襲的呼吸測定方法としては、自己参照型微小電極(self-referencing microelectrode)やクラーク型酸素センサーを用いた胚の呼吸量測定が報告されている⁹⁾¹⁰⁾。筆者らは、局所領域における生物反応を電気化学的に高精度で検出する有効な技術である電気化学的イメージング法に注目し、この技術の中心となる走査型電気化学顕微鏡(SECM)をベースに、「受精卵呼吸測定装置(細胞呼吸測定システム)」を開発している¹⁾¹¹⁾。さらに、センサープローブの高感度化や非侵襲性測定液を開発することで、単一の卵子の呼吸量

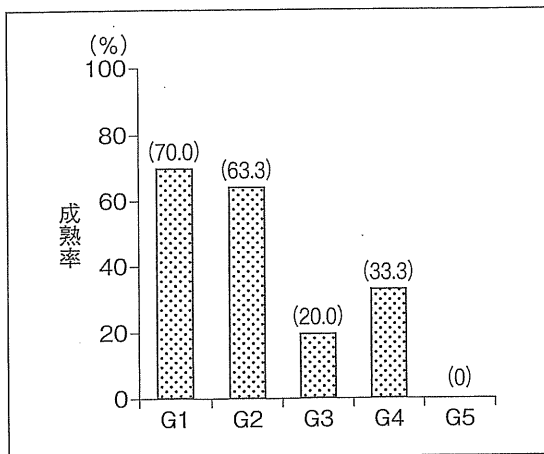


図4 COCを成熟培養した後の卵子成熟率
G1:グレード1, G2:グレード2, G3:グレード3, G4:グレード4, G5:グレード5。

を高精度で測定することができることが可能になってきた¹²⁾。

現在、胚の品質（クオリティー）は、割球などの数や形態を指標とする形態観察による評価が一般的である。しかしながら、評価の基準となる形態的特徴は定量性に欠けるため、判定結果が観察者の主観に左右され、評価の精度に影響が出る可能性がある。これまでに、胚の客観的評価のための様々な手法が検討されてきた。例えば、胚の代謝に注目した評価法として、胚の代謝活性をグルコース、ピルビン酸、アミノ酸などの栄養素の消費に着目した研究がある^{13)~17)}。また、ミトコンドリアは酸化リン酸化反応（呼吸）により細胞活動に必要なエネルギー（ATP）を産生し、胚の発生などに密接に関与していることから、細胞の酸素消費量測定によって胚の品質を評価する方法も試みられてきた⁷⁾⁹⁾。

一方筆者らは、詳細な胚の微細構造観察によりミトコンドリアの発達と胚の品質がリンクしていることを発見し、呼吸活性を指標とする胚品質評価法を提案してきた¹⁸⁾。前述の「受精卵呼吸測定装置」を用いて、家畜や実験動物を中心に呼吸能を指標とする品質評価の有効性に関して興味深い知見が得られている。ウシでは桑実胚期において高い呼吸活性を有する胚の多く

は、呼吸測定後に追加培養を行うと高い確率で品質良好な胚盤胞へと発生する¹²⁾。また、凍結時に呼吸量の大きい胚盤胞は、融解した後の生存率も良好であるという結果が得られている¹⁹⁾。さらに、呼吸測定後の胚を借腹牛に移植し胚の呼吸活性と受胎率の関係を調べた結果、移植前の呼吸量が基準値以上（胚盤胞で $1.0 \times 10^{14}/\text{mol} \cdot \text{sec}^{-1}$ 、初期胚盤胞で $0.8 \times 10^{14}/\text{mol} \cdot \text{sec}^{-1}$ 、桑実胚で $0.5 \times 10^{14}/\text{mol} \cdot \text{sec}^{-1}$ ）の胚を移植した場合、60%以上の高い妊娠率が得られている¹²⁾²⁰⁾。

これら動物実験の結果を踏まえ、ヒト胚のクオリティー評価と不妊治療における臨床応用を目的として「受精卵呼吸測定装置」の探索的臨床研究を試みている。ヒト胚の形態的クオリティーと呼吸能との関連を調べた結果、Veeck分類によるグレードと胚の呼吸能との間には明確な相関は認められないが、胚の呼吸能と胚盤胞発生率に興味深い関係が認められている²¹⁾。媒精3日目（day 3）の胚を呼吸量（ $\times 10^{14}/\text{mol} \cdot \text{sec}^{-1}$ ）を基準に、 >0.26 、 $0.26 \sim 0.56$ 、 <0.56 の3グループに分け、それぞれ胚の追加培養を行った結果、 $0.26 \sim 0.56$ の範囲の呼吸量を示した胚の65.8%が胚盤胞に発生し、他のグループと比較して最も高い胚盤胞発生率を示した。この結果は、呼吸活性値がある一定の範囲内にあるヒト分割胚は高い発生能を有するクオリティー良好胚であることを示している。さらに呼吸計測の有効性を調べるために、患者の同意を得た上で呼吸測定した胚の移植を行った。Veeck分類で同じグレードの胚が複数得られた症例において、形態的グレードと呼吸活性が最も良好な胚を移植した場合、従来の形態的評価のみで選別した胚を移植した場合と比べて妊娠率が優位に向上するという結果が得られている²²⁾。このように、臨床レベルにおいても呼吸活性を指標とする胚品質評価の有用性が示されてきている。

本症例では「受精卵呼吸測定装置」を用いて、初めて単一ヒトCOCの呼吸量測定に成功し、COCの呼吸量活性と卵子成熟能の関係を示唆

する結果が示された。卵子は単一細胞であるため、胚のように割球数やその形態を基準にクオリティーを評価することは困難である。しかし、卵子のクオリティーを卵丘細胞の状態から評価しようとする試みがある。採卵時に回収された顆粒膜細胞のアポトーシス小体の出現率が低い卵胞から得られた卵ほどクオリティーが良好であると報告している²³⁾。最近筆者らは、IVM-IVF (in vitro maturation and in vitro fertilization) 施行時に、COCにおいて卵子面積 (oocyte-area), 卵子円形率 (oocyte-circularity), 卵丘細胞の多層形成 (cumulus-layer), 卵丘細胞-卵子面積比 (C-ratio) などを画像解析ソフト (NIH Image) により解析し、これら計測値を指標に COC の段階で卵子成熟率の予測が可能かどうか検討している。これまでに、成熟培養 26 時間前後において C-ratio が大きい、すなわち卵丘細胞が多く付着している COC は高い卵子成熟率を示すことを明らかにしている²⁴⁾。本研究では、卵丘細胞の数と付着状態と COC の呼吸活性および卵子成熟率の関係を調べた結果、卵子成熟率と呼吸量は付着している卵丘細胞の数にほぼ比例することが明らかになった。さらに、卵子成熟率と呼吸活性が両方とも最も高いグレード 1 では、卵子と卵丘細胞間のギャップ結合の発達が非常に顕著であり、他のグレードの COC と比べて卵丘細胞内のミトコンドリアもよく発達していた。このように、卵丘細胞の呼吸活性は卵丘細胞-卵子間相互作用と卵子のクオリティーと密接に関連していることから、COC の呼吸測定は卵子のクオリティーを COC の段階で早期に評価できる画期的な方法となる可能性がある。

おわりに

本症例では、SECM を用いた電気化学計測技術は、ヒト COC のミトコンドリアの呼吸機能解析に有効であること、また、これまで困難であった COC 内の卵子の品質を呼吸活性を指標に評価できる可能性が示された。電気化学計測技術は、非侵襲・高感度測定法であることから、

ヒト胚や卵子の品質評価など不妊治療における臨床応用が十分に期待できる。

文 献

- 1) Abe H : A non-invasive and sensitive method for measuring cellular respiration with a scanning electrochemical microscopy to evaluate embryo quality. *J Mamm Ova Res* 24 : 70-78, 2007
- 2) Mills RM et al : Oxygen consumption of pre-implantation mouse embryos. *Exp Cell Res* 47 : 337-344, 1967
- 3) Magnusson C et al : Oxygen consumption by human oocytes and blastocysts grown in vitro. *Hum Reprod* 1 : 183-184, 1986
- 4) Magnusson C et al : Oxygen consumption of maturing rat oocytes. *Biol Reprod* 17 : 9-15, 1977
- 5) Nilsson B et al : Correlation between blastocyst oxygen consumption and trophoblast cytochrome oxidase reaction at initiation of implantation of delayed mouse blastocysts. *J Embryol Exp Morphol* 71 : 75-82, 1982
- 6) Houghton FD et al : Oxygen consumption and energy metabolism of the early mouse embryo. *Mol Reprod Dev* 44 : 476-485, 1996
- 7) Thompson JG et al : Oxygen uptake and carbohydrate metabolism by in vitro derived bovine embryos. *J Reprod Fertil* 106 : 299-306, 1996
- 8) Donnay I et al : Embryo metabolism during the expansion of the bovine blastocyst. *Mol Reprod Dev* 53 : 171-178, 1999
- 9) Trimarchi JR et al : Oxidative phosphorylation-dependent and independent oxygen consumption by individual preimplantation mouse embryos. *Biol Reprod* 62 : 1866-1874, 2000
- 10) Lopes AS et al : Respiration rates of individual bovine in vitro-produced embryos measured with a novel, non-invasive and highly sensitive microsensor system. *Reproduction* 130 : 669-679, 2005
- 11) Shiku H et al : Oxygen consumption of single bovine embryos probed with scanning electrochemical microscopy. *Anal Chem* 73 : 3751-3758, 2001
- 12) Abe H et al : In vitro culture and evaluation of embryos for production of high quality bovine embryos. *J Mamm Ova Res* 21 :

- 22-30, 2004
- 13) Overstrom EW : In vitro assessment of embryo viability. *Theriogenology* 45 : 3-16, 1996
 - 14) Rieger D et al : Developmentally related changes in the uptake and metabolism of glucose, glutamine and pyruvate by cattle embryos produced in vitro. *Reprod Fertil Dev* 4 : 547-557, 1992
 - 15) Rieger D : Relationship between energy metabolism and development of early mammalian embryos. *Theriogenology* 37 : 75-93, 1992
 - 16) Rieger D et al : Changes in the metabolism of glucose, pyruvate, glutamine and glycine during maturation of cattle oocyte in vitro. *J Reprod Fertil* 100 : 257-262, 1994
 - 17) Gopichandran N et al : Metabolic characterization of the bovine blastocyst, inner cell mass, trophectoderm and blastocoel fluid. *Reproduction* 126 : 299-308, 2003
 - 18) Abe H et al : Evaluation of bovine embryos produced in high performance serum-free media. *J Reprod Dev* 49 : 181-192, 2003
 - 19) Shiku H et al : Metabolic and enzymatic activities of individual cells, spheroids and embryos as a function of the sample size. *Sens Actuat B* 108 : 597-602, 2005
 - 20) Abe H et al : Evaluating the quality of individual embryos with a non-invasive and highly sensitive measurement of oxygen consumption by scanning electrochemical microscopy. *J Reprod Dev* 52 (Suppl) : S55-S64, 2006
 - 21) Utsunomiya T et al : Evaluating the quality of human embryos with a measurement of oxygen consumption by scanning electrochemical microscopy. *J Mamm Ova Res* 25 : 2-7, 2008
 - 22) 後藤香里ほか : 選択的単一胚移植 (eSET) における移植胚選別困難例に対する呼吸量測定の有用性. *産婦の実際* 59 : 1277-1281, 2010
 - 23) Nakahara K et al : The incidence of apoptotic bodies in membrane granulosa can predict prognosis of ova from patients participating in vitro fertilization programs. *Fertil Steril* 68 : 312-317, 1999
 - 24) Murakawa H et al : Morphological evaluation and measurement of the respiration activity of cumulus-oocyte complexes to assess oocyte quality. *J Mamm Ova Res* 26 : 32-41, 2009

特集

卵子のエイジング III. 胚の非侵襲的評価法

10. 体外培養卵子の評価—臨床応用

よしだ ひろおき *1・たなか たかゆき *1・あべ ひろゆき *2
 吉田仁秋*1・田中孝幸*1・阿部宏之*2
 吉田レディースクリニックARTセンター*1
 山形大学大学院理工学研究科*2

要旨

走査型電気化学顕微鏡 (SECM) はミトコンドリア機能とヒト卵子, 胚のクオリティー機能の関係を評価する有益な装置である. 体外培養卵子の評価法としてわれわれは SECM を用いてヒト IVM 卵子や胚の呼吸量を測定し検討した. ヒト卵子は MII 期卵に成熟することによりその呼吸量を維持し, 受精後呼吸活性はさらに上昇し, 桑実胚から胚盤胞で最大となる. IVM 由来卵と COH 由来卵において両者の呼吸量に有意差を認めず, さらにその後の胚発生においても同様の結果が得られた. このことは IVM 由来卵子も受精卵となればその後の胚発生は呼吸量からも同様の機能を有することが示唆された.

Key Words IVM 卵子, 胚の品質, 酸素呼吸量

1978年 Edward が世界で初めて体外受精を成功させ, 昨年ノーベル賞を受賞したことは記憶に新しい. この間体外受精も排卵誘発法や培養液の開発が進み胚盤胞まで培養が可能となり, 患者に負担の少ないかつ妊娠率の損なわない誘発法等が開発されてきた¹⁾. 多嚢胞性卵巣症候群 (polycystic ovary syndrome: PCOS) は無排卵あるいは稀発月経を呈する症候群で卵胞が多数存在するため, 誘発により卵巣過剰刺激症候群 (ovarian hyper stimulation syndrome: OHSS) を引き起こすこととなり注意を要する. そこで低刺激周期の誘発方法や無刺激により未熟卵を回収し, 体外で成熟させ受精卵を移植する方法 IVM-IVF ET (in vitro maturation, in vitro fertilization & embryo transfer) が開発された. この IVM は妊娠率の上昇とともに ART (assisted reproductive technology) にも急速に取り入れら

れ, 最近のデータでは従来から行われている通常の体外受精とほぼ同様な有用性と安全性も報告されている¹⁾.

卵子や胚の形態学的評価はその精度を高めるため, 非侵襲的な卵子や胚評価のため様々なアプローチがなされてきた²⁾. ミトコンドリアは呼吸により細胞活動に必要な ATP を産生する重要な細胞小器官であり, 酸素消費と密接な関係があることを山形大学の阿部らは報告している³⁾⁴⁾. その報告によると, 様々な動物種の胚の研究においてミトコンドリアが正常に発達している胚は, 高い品質の良好胚であるとしている. これらの観点から卵子や胚の品質管理として, 走査型電気化学顕微鏡 (SECM) が開発され, 呼吸測定装置は安全で, 簡便かつ精度の高い客観的評価可能な装置である.

今回われわれはヒト未成熟卵の呼吸量測定を

この SECM を用いて施行し、ヒト未受精卵や卵子-卵丘細胞複合体 cumulus oocyte complex (COC) の呼吸量を測定し、その電顕的な超微形態を観察し、胚評価法として有用か検討した。さらにその後発生した胚の呼吸量について検討してきたのでその概要を報告する。

当院における治療成績

当院での2009年までの治療成績(表1)および当院でのプロトコルを(図1)に示す。2004年の妊娠率と比較し約2倍の29%と上昇している。これは成熟培養液の開発や技術の進

表1 IVM-IVF成績(2007年4月~2009年9月)

パラメーター	結果	範囲	妊娠
年齢(y)	30.0±4.9*	25-34	32.0±3.2
ΣFSH(IU)	354±265*	0-750	330±265
ピークE ₂ (pg/mL)	216±315*	64-783	220±185
採卵日	11**	8-12	11
hCG投与例(%)	93.7		95
採卵数	6**	1-17	10.4±5.3
成熟率(%)	62.8	0-100	54.7
受精率(%)	63.8	0-100	85.8
移植胚数	1.3±0.7*	1-2	2
キャンセル率(%)	18.7		
臨床的妊娠率/胚移植(%)	27.3		
融解周期	11.6		
流産率(%)	22.2		

Values are expressed as mean±SD (*) or medians (**)

Mann-whitney's U test.

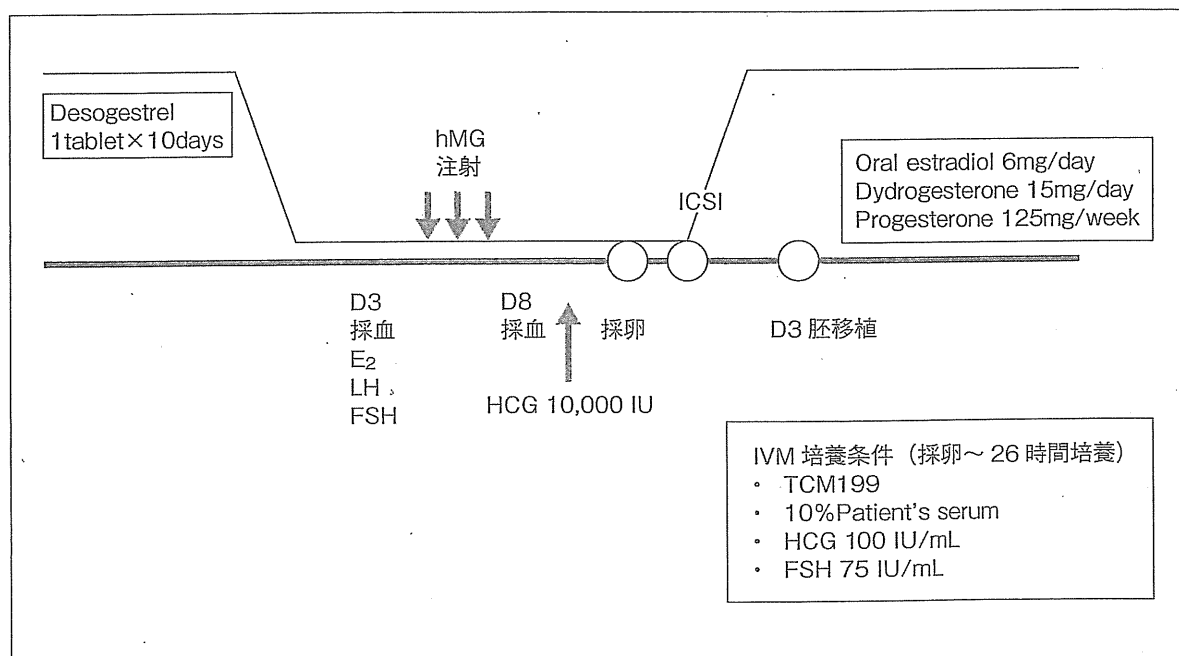


図1 IVM-IVFプロトコル

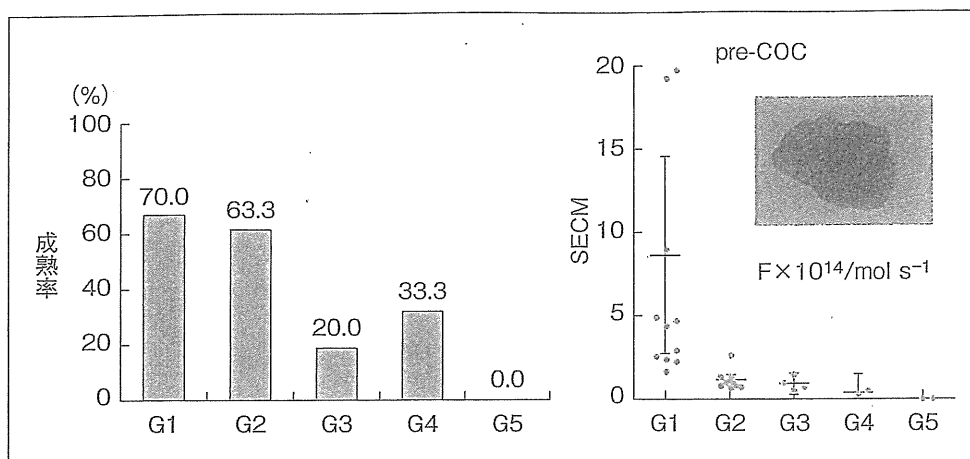


図2 ヒト未成熟卵の成熟率と酸素呼吸量

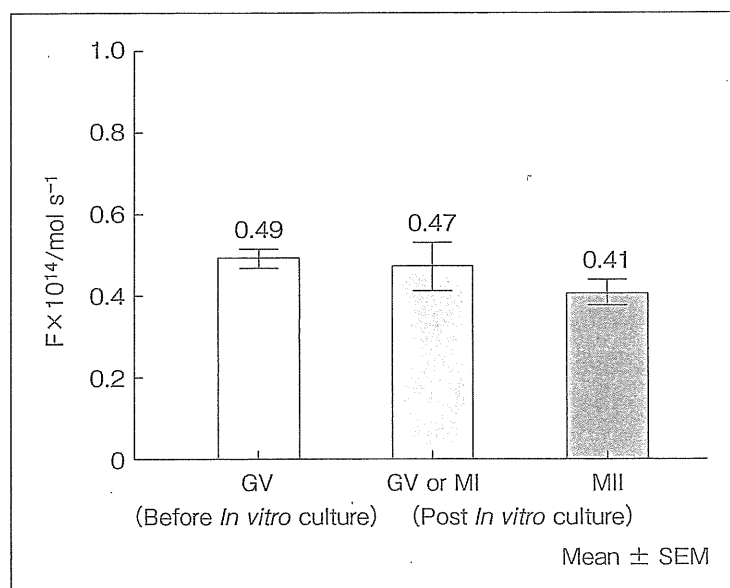


図3 ヒト未成熟卵の酸素呼吸量

歩等のためと考えられる。しかしながら成熟率や受精率は controlled ovarian hyperstimulation (COH) と比較し未だ低値でさらなる改善が必要であり、今後妊娠率の向上を目指し、排卵誘発法の検討、培養液や技術の改良、着床率の改善を検討する必要がある。

卵子卵丘細胞複合体 (COC) および未成熟卵の呼吸量

今回われわれは IVM-IVF にて採取された

COC および未成熟卵を形態学的に分類すると、Grade 1 は 4 層以上に重なる卵丘細胞と均等円形卵子、Grade 2 は 3 層に重なり合う卵子全体を覆う卵丘細胞 Grade 3 は卵丘細胞に覆われる領域が半分以下 Grade 4 は完全裸化卵子 (卵丘細胞なし) Grade 5 は卵子が小さいもしくは変形したものとした。これらの形態学的分類によるヒト卵子成熟率は Grade 1 で 70.0%、Grade 2 で 63.3%、Grade 3 で 20.0%、Grade 4 で 33.3%、Grade 5 で 0% と、Grade の下降に

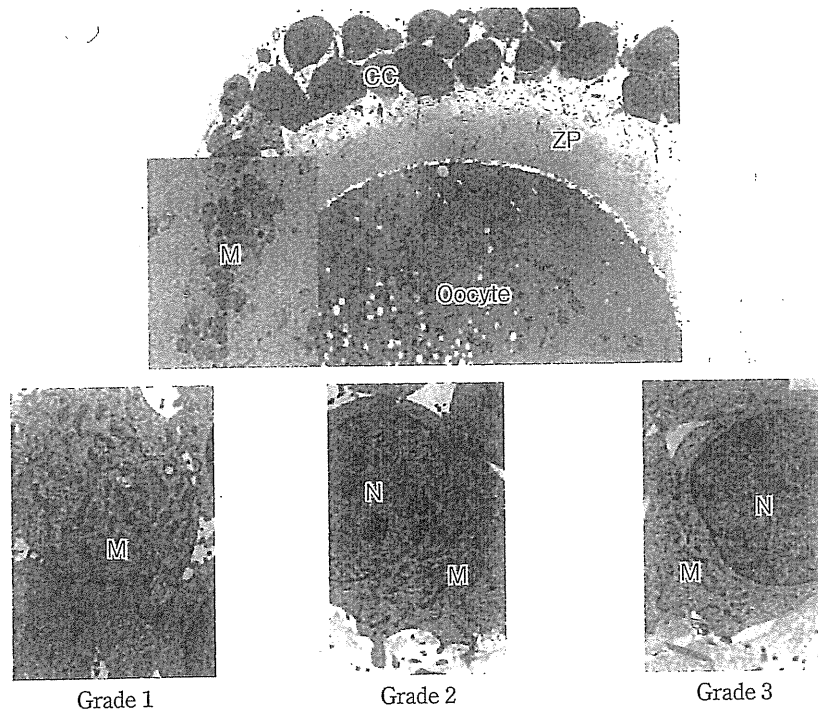


図4 ヒト卵子-卵丘細胞複合体 (COC) の微細構造

伴って成熟率も減少した (図2)。

IVM26時間培養前のヒトCOC全体の呼吸量は平均値は $4.17 \pm 1.18 \text{ F} \times 10^{14} / \text{mol S}^{-1}$ であった。IVM培養前のGrade分類による酸素呼吸量の比較では、培養前後ともにGradeの下降とともにその酸素呼吸量は減弱した。図3はヒト卵子IVM卵とCOHによる卵子の呼吸量を示す。GV期の平均値は $0.49 \text{ F} \times 10^{14} / \text{mol S}^{-1}$ GV期もしくはMI期で $0.47 \text{ F} \times 10^{14} / \text{mol S}^{-1}$ MII期で $0.41 \text{ F} \times 10^{14} / \text{mol S}^{-1}$ となり統計学的に有意差を認めなかった。

透過型電子顕微鏡 (TEM) を用いたヒトCOCおよび未成熟卵子の電子顕微鏡像

ヒト未成熟卵を採取し、卵丘細胞、未成熟卵子の微細構造を透過型電子顕微鏡 (TEM) を用いて観察評価した (図4)。上段はGrade1のヒト卵子-卵丘細胞複合体の微細構造を示し、内側 (Oocyte) は卵細胞質で卵細胞質内に矢印で

示したようにミトコンドリアが観察される。数も豊富で円形の丸いミトコンドリアの拡大像が左側である。下段はGrade別のヒト卵丘細胞の微細構造で、Grade1はミトコンドリアの発達が著明で数も豊富で cristae 形成も一部散見される。Grade2,3になるに従ってミトコンドリアの数も減少し、疎になり、ミトコンドリアの形状も縮小傾向を示した。この研究により卵丘細胞の豊富な卵子ほどミトコンドリアの発達が顕著であり、かつ酸素呼吸量もGradeのよいものほど高くなり、細胞内のミトコンドリア量と酸素呼吸量が正の相関を示すことが判明した⁶⁾ (図2)。

ヒトIVMおよびCOH分割胚の酸素呼吸量

ヒト受精卵の酸素呼吸量の測定はIVM由来受精卵では平均 $0.40-0.50 \text{ F} \times 10^{14} / \text{mol S}^{-1}$ とCOHの受精卵と同様の結果を得た。さらに受精卵の酸素呼吸量もそれぞれ初期分割胚の平均

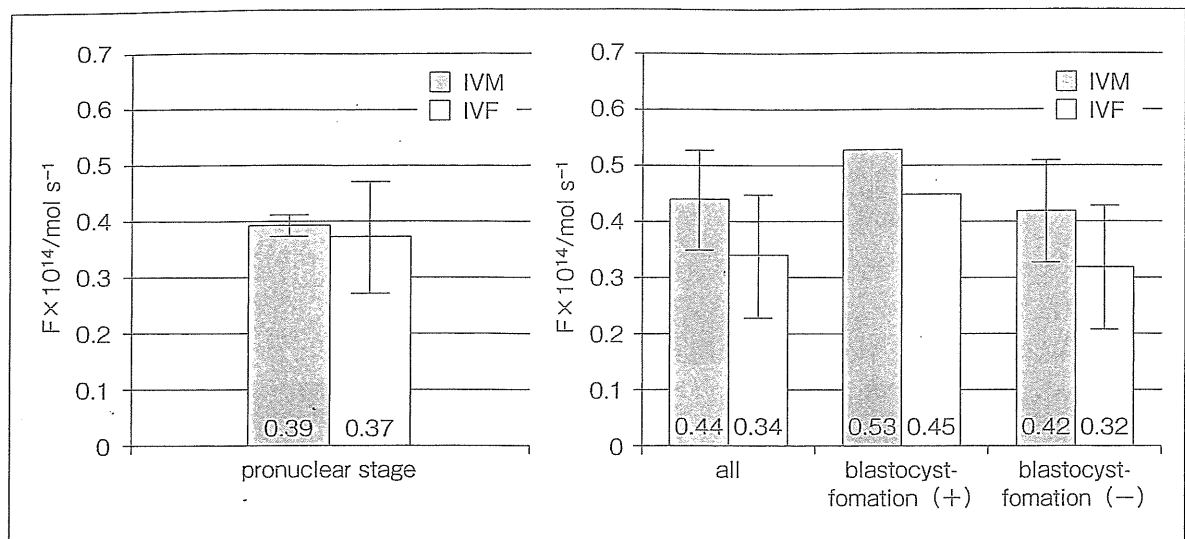


図5 受精卵（前核期・Day 3）の酸素呼吸量の比較

酸素呼吸量は4細胞期6細胞期8細胞期および10細胞期でそれぞれ 0.34 ± 0.1 , 0.37 ± 0.1 , 0.4 ± 0.2 , 0.50 ± 0.2 ($F \times 10^{14} / \text{mol S}^{-1}$) である。D-3の分割胚では同じWeek分類のGradeの胚でも個々の分割胚によって酸素呼吸量が異なった。COH胚とIVM胚との両方で相違を認めなかった。すなわちD3の分割胚での比較ではIVM 0.44 ($F \times 10^{14} / \text{mol S}^{-1}$), COH 0.34 ($F \times 10^{14} / \text{mol S}^{-1}$) で胚盤胞発生したものは呼吸率に高い傾向を認めたが有意差を認めなかった(図5)。この結果は、ヒト分割胚はある一定の最適な酸素呼吸量の範囲があり、その後の胚発生は予測可能であることが示唆された。

考 察

卵子や胚の品質評価として形態学的手法が長く用いられてきた。しかし形態学のアプローチのみではその後の胚発生や妊娠率の精度を上昇させることが困難な場合も経験する。そこで卵子や分割胚の品質評価のため、胚の代謝活性をグルコース、ピルビン酸、アミノ酸等の栄養素の消費に着目した研究もなされた⁷⁾。細胞の呼吸(酸素消費)は酸化的リン酸化の過程で

ATPを産生し、酸素消費を起こし、これも胚の代謝活性の評価の一つとされる⁸⁾。

近年胚の新しい評価法として培養24時間後の前核の核小体の配列により胚盤胞への発生率と着床率の改善例がTesarikらにより報告されたが⁹⁾、最近の見尾らのtime-lapse cinematographyを用いた報告では、核小体の配列も個々の分割卵で様々に移動し、動態的観察では核小体の配列はある一時点での評価の一部にすぎないことが判明した¹⁰⁾。すなわち核小体は発育の過程で配列をドラマチックに変えている。

最初のマウス胚盤胞とヒト卵、胚盤胞の測定は¹¹⁾酸素ヘモグロビンからヘモグロビンへの変換による酸素呼吸量を間接的に計測した。その後哺乳類胚の酸素呼吸量は様々な代謝過程の情報をパラメーターとしてCartesinのようにdiverを用いたり¹²⁾、電気化学的方法などにより計測された¹³⁾。より正確で簡便な酸素呼吸量の測定が求められ、単一の酸素呼吸量の測定が可能な方法が開発された¹⁴⁾。この単一胚の測定可能なシステムは底辺を円錐状に工夫したmicrowellの使用により電気化学顕微鏡のスキャンを可能にした³⁾⁴⁾。このシステムの使用により単一細胞の呼吸量測定が可能になった。

阿部らの報告によると、多くの動物胚では桑実期から胚盤胞に期にかけて呼吸量の増加とミトコンドリアの発達が一致して起こり、呼吸量の高い胚は発生能や耐凍能が良好である。さらに呼吸量測定後の移植実験では基準値以上の呼吸量を示す胚は妊娠率が高いことが判明した。よって呼吸量測定は胚の品質評価に有効である。ヒト胚では同じWeek分類のGradeでも呼吸量が個々の胚の品質により異なるが、胚分割には最適な酸素呼吸量を必要とし、一般に桑実期胚や胚盤胞期にその呼吸量は上昇した。

ヒト受精卵においてIVM卵、COH卵でも卵の質は個々の個体差が大きいが、その後の胚発生に最適な酸素呼吸量の範囲があることが判明した。さらに初期分割胚、桑実胚、胚盤胞と酸素呼吸量は次第に上昇し、胚盤胞で最も上昇していた。これらの結果はウシやブタなどの他の動物種と同様な結果を示した⁴⁾。さらに形態学的評価と呼吸量を組み合わせると妊娠率が上昇すると最近報告されている。

さらに卵丘細胞の付着状態によって卵子の呼吸能が異なり、高い呼吸活性を有するCOCは卵子成熟培養後の成熟率が高いことが判明した。ヒト卵子の呼吸量も同様に卵丘細胞の付着3層以上のGrade 1, 2では有意に呼吸量は高く、その後の成熟率にも反映され、受精率や胚発生率に影響を与えることが判明した。

● 文 献

- 1) Jin-Ho Lim, RC Chian, et al : Selection of patients for natural cycle in vitro fertilization combined with in vitro maturation of immature oocytes. *Fertil Steril* 2009 ; 91 : 1050-1055.
- 2) Boiso I, Veiga A, Edwards RG, et al : Fundamentals of human embryonic for growth in vitro and the selection of high-quality embryos for transfer. *Reprod. Biomed. Online* 2002 ; 5 : 328-350.
- 3) Abe H, Shiku H, Aoyagi S, Matsue T, Hoshi H, et al : Respiration activity of bovine embryos cultured in serum-free and serum-containing media. *Reprod. Fertil. Develop* 2005 ; 17 : 205.
- 4) Abe H, et al : A non-invasive and sensitive method for measuring cellular respiration with a scanning electrochemical microscopy to evaluate embryo quality, *J. Mamm. Ova. Res* 2007 ; 24 : 70-78.
- 5) Utsunomiya T, Goto K, Nasu M, Kumasaki Y, Araki Y, Yokoo, Sasaki T, Abe H, et al : Evaluating the quality of human embryos with a Measurement of oxygen consumption by scanning electrochemical microscopy, *J. Mamm. Ova. Res* 2008 ; 25 : 2-7.
- 6) H Murakawa, H Yoshida, et al : Morphological Evaluation and Measurement of the Respiration Activity of Cumulus-oocyte complexes to Assess oocyte Quality. *Reproductive Research Center Yoshida Ladies Clinic Sendai Japan, J. Mamm. Ova Res* 2009 ; 26 : 32.
- 7) Rieger D, Loskutoff NM, et al : Changes in the metabolism of glucose, pyruvate, glutamine and glycine and glycine during maturation of cattle oocyte in vitro, *J. Reprod. Fertil* 1994 ; 100 : 257-262.
- 8) Thompson J G, Partridge R J, Houghton F D, Cox C I, Leese H J, et al : Oxygen up take and carbohydrate metabolism by in vitro derived bovine embryos, *J. Reprod. Fertil* 1996 ; 106 : 299-306.
- 9) Tesalik J, Junca A M, Hazout A, Aubriot F X, Nathan C, Cohen-Bacrie P, Dumont-Hassan M, et al : Embryos with high implantation potential after intracytoplasmic sperm injection can be recognized by a simple, non-invasive examination of pronuclear morphology, *Hum. Reprod* 2000 ; 6 : 1396-1399.
- 10) Mio Y, et al : Morphological analysis of human embryonic development using time lapse cinematography, *J. Mamm. Ova. Res* 2006 ; 23 : 27-35.
- 11) Nilsson B, Magnusson C, Wideha S, Hillensjo T, et al : Correlation between blastocyst oxygen consumption and trophoblast cytochrome oxidase reaction at initiation of delayed mouse blastocysts, *J. Embryol. Exp. Morphol* 1982 ; 71 : 75-82.
- 12) Millis RM, Brinster RL, et al : Oxygen consumption of pre-implantation mouse embryos. *Exp. Cell Res* 1967 ; 47 : 337-344.
- 13) Overstorm EW, Duby RT, Dobrinsky J, Roche JF, Boland MP, et al : Viability and oxidative metabolism of the bovine blastocyst, *Theriogenology* 1992 ; 37 : 269.
- 14) Shiku H, Shiraishi T, Aoyagi S, Utsumi Y, Matsudaira M, Abe H, et al : Respiration activity of single bovine embryo entrapped in a cone-shaped microwell monitored by scanning electrochemical microscopy, *Anal. Chem.* 2004 ; 76 : 51-58.

著者連絡先

〒982-0817
宮城県仙台市太白区西中田二丁目23-5
吉田レディースクリニック ART センター
吉田仁秋